

# **Effects of Subsurface Fracture Interactions on Surface Deformation**

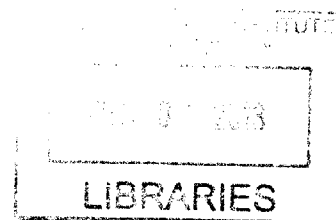
by

Ruel Jerry

B.S. Physics (2010)

Howard University

ARCHIVES



SUBMITTED TO THE DEPARTMENT OF EARTH, ATMOSPHERIC AND  
PLANETARY SCIENCES IN PARTIAL FULFILLMENT OF THE REQUIREMENTS  
FOR THE DEGREE OF

MASTER OF SCIENCE IN GEOPHYSICS  
AT THE  
MASSACHUSETTS INSTITUTE OF TECHNOLOGY

SEPTEMBER 2013

© 2013 Massachusetts Institute of Technology  
All rights reserved

Signature of Author.....

Department of Earth, Atmospheric and Planetary Sciences  
August 26, 2010

Certified by.....

Bradford Hager  
Cecil and Ida Green Professor of Geophysics  
Thesis Supervisor

Accepted by.....

Robert Van der Hilst  
Schlumberger Professor of Earth Sciences  
Department Head of Earth, Atmospheric and Planetary Sciences

# **Effects of Subsurface Fracture Interactions on Surface Deformation**

by

Ruel Jerry

Submitted to the Department of Earth, Atmospheric and Planetary Sciences in Partial Fulfillment of the Requirements for the Degree of Master of Science in Geophysics

## **ABSTRACT**

Although the surface deformation resulting from the opening of a single fracture in a layered elastic half-space resembles the observed deformation at the InSalah site, it seems unlikely that only a single fracture is involved. This raises the question of how interaction among multiple fractures affects surface deformation. Finite element modeling is used to build a 3D model of a reservoir with multiple fractures. The interacting cracks and fractures give this model a more complicated stress state, and so any surface deformation would be different from that of a model with a single fracture.

Geodetic monitoring of large-scale CO<sub>2</sub> sequestration provides a potentially powerful and cost-effective tool for interrogating reservoir structure and processes. For example, InSAR observations at the InSalah, Algeria sequestration site have mapped the surface deformation above an active reservoir, and helped delineate the effects of CO<sub>2</sub> storage.

The impact of interactions on individual fractures and the qualitative changes in the surface displacement and stress fields are considered and the importance of orientation, position and fracture area is investigated. It was found that when the crack locations are biased towards stacked parallel arrangements, then the shielding effect of interactions dominates, meaning that the overall stiffness of a representative volume increases. When collinear interactions dominate then the overall stiffness is reduced. These effects are then used to find a volume average and a continuum description of a solid with effective elastic properties. In this way a volume of fractured rock can be replaced with a representative volume with elastic properties that approximate the interaction effects.

Thesis Supervisor: Bradford Hager  
Title: Cecil and Ida Green Professor of Geophysics

## ACKNOWLEDGEMENTS

This has been an incredible three-year experience, with many highs and many lows. I certainly would not have been able to survive the lows if not for a great deal of people who have supported me this far and provided all of the highs. I would like to acknowledge some of them in the knowledge that out of necessity I am omitting many more people who have played an important role in my experience. If I was able to mention everyone that needed to be mentioned I would never stop writing.

I would like to thank the Earth Resources Lab for the opportunity to conduct research at MIT; this has been an amazing chapter that will stay with me for my entire life. The support and encouragement that I received from every member of the lab was invaluable to me, especially when my projects were not progressing the way I would have liked. In particular I need to mention the two people who were my advisors during my time here, Professor Brad Hager and Professor Dale Morgan. Brad was my primary advisor and was a very supportive influence. I tend to be wry, so it was good to have an advisor who was often on the same page. My one regret was that we never got a chance to go kayaking as we had planned. As a moderately good kayaker, I would have benefited from expert kayaking advice, but I will have to make do with his advice on geomechanics. As a fellow Trinidadian, Dale's advice (solicited and otherwise) on work, philosophy and life was always first-rate. His life lessons were always something to look forward to. His input was one of the main reasons that I decided to go to MIT in the first place, and I still have no regrets three years later.

There were many other important members of ERL that shaped my experience here. I must thank Anna Shaughnessy, Sue Turbak, and Terri Macloon for all their help and support. Anna has given me very good career advice; Sue and Terri have been ever-present forces for good in ERL. Faculty like Alison Malcolm, Tom Herring, Rob Van der Hilst and Taylor Perron were also very important to my growth as a geophysicist. Alison and Taylor gave me great advice on my projects, particularly before my Generals Exam. I took classes given by Tom and Rob and they have both shaped the way I approach geophysical problems.

I would like to thank all of my fellow travellers at ERL for their support. They were great

resources when I needed help or just to vent. I need to single out Yulia Agramakova, Sudhish Bakku, Scott Burdick, Hussam Busfar, Martina Coccia, Thomas Gallot, Chen Gu, Clarion Hess, Bongani Mashele, Gabi Melo, Nasruddin Nazerali, Beebe Parker, Alan Richardson, Sedar Sahin, Andrey Shabelansky, Haoyue Wang, Lucas Willemsen, Di Yang, and Ahmad Zamanian. Yulia, Nas and Bongani were my comrades at arms in the Morgan lab and were absolutely vital in their role as buffers when I was in trouble. Martina and Sedar were the people that I entered MIT with and I will miss eating Turkish food with Sedar and being stranded in Iceland with Martina. Lucas is always a smiling, happy presence, even when there is no warrant, yet somehow this is not grating. I still don't understand how that is. Gabi is borderline therapeutic and I will miss tolerating her odd affection for heavy metal music. Scott is one of the best drinking partners I have ever had. Banter with Sudhish and Di is always a highlight of a sleepy workday.

I made some amazing friends at EAPS that I also need to single out. They were responsible for making the last three years some of the most fun I have ever had. In particular, Daniel Amrhein, Alexandra Andrews, Annie Bauer, Rene Boiteau, Sara Bosshart, Stephanie Brown, Eric Brugler, Frank Centinello, Deepak Cherian, Veronique Dansereau, Andrew Davis, Mike Eddy, Alex Evans, Helen Feng, Mike Floyd, Kyrstin Fornace, Kate French, Sarvesh Garimella, Aimée Gillespie, Marie Giron, Niya Grozeva, Nick Hawco, Jordon Hemingway, Peter James, Christopher Kinsley, Ben Klein, Yavor Kostov, Izi Le Bras, Ben Mandler, Peter Meleney, Steve Messenger, Andy Miller, Patrick Mitchell, Melissa Moulton, Sharon Newman, Jaap Nienhaus, Jean-Arthur Olive, Alejandra Quintanilla, Paul Richardson, Sarah Rosengard, Kat Saad, Michael Manuel Sori, Oscar Sosa, Elena Steponaitis, Matthieu Talpe, Yodit Tewelde, Sonia Tikoo, Asa Trapp, Phil Wolfe, and many more.

Rene has been the best friend anyone could ask for when they need cheering up. I will miss visiting his family for Thanksgiving and just randomly going to his house when I'm in a bad mood. My roommates Yodit and Alex made the Black Hole a fantastic place to live. Arthur, despite his overwhelming Frenchness, remains one of the first people I call when I need anything, except for restraint. Sara remains the classiest person I know. Mike Sori is Mike Sori. I don't know anyone with more mental fortitude than Frank; I will definitely miss rum nights with him. Peter Meleney is a great resource to have

around, in good times and bad; I will miss harassing him. Annie and Asa do a great job dealing with my more curmudgeonly behavior, as does Alex Andrews; I will miss going up to Annie's office in the middle of the workday when I need to slack off. Helen was the first person I made friends with at EAPS and remains one of my best. Jordon has managed to become one of my closest friends here, despite having been brainwashed by UC Berkeley; that's an accomplishment. Abuelita Alejandra is the elder voice of wisdom. Kyrstin and Nick took me in at Woods Hole whenever I needed to escape from Cambridge and MIT. Beebe and Matthieu are always on the same page that I am on, regardless of how absurd I am. Dan and Melissa are the most patient people in the world for putting up with me. Elena and Jaap are the nicest people in the world. I'll miss playing badminton with Deepak, smoking cigars with Paul, tasting wine with Ben Mandler, and scowling with Ben Klein. I braved the Boston Marathon bombings with Mike Eddy, 2 blocks away from the finish line (Boston Strong!).

Outside of EAPS, my first roommate Daniel Soltero was a great person to enter MIT with. I will miss practicing my Spanish and eating too much adobo. Erika Sandford and Orrin Barnhart were also great roommates; nicer people don't exist. I will certainly miss watching soccer with Joel Batson and letting him know why the team he supports is terrible. I will also miss Esther Raymond and Donnell Jones, beating them at soccer is as satisfying as it is routine. Phil Muñoz, who is one of the smartest, most dignified people in the world. Nancy Guillen and Indira Deonandan could always keep me grounded.

I also need to acknowledge the MIT Summer Research Program, MSRP, with whom I did a summer internship. During this program I realized that I wanted to go to MIT for graduate school, and Dean Christopher Jones and Monica Orta, or as we affectionately called her, **Momica**, are two driven brilliant people who have crafted a superb program that has done a lot for a lot of future scientists and engineers. Professor Janet Conrad at MIT's Physics department, and Professor Lindley Winslow, now at UCLA, were integral to my development as a scientist.

Last but not least, I need to thank my family, who has been supportive throughout my career. I am grateful to my parents for their support and interest. My sister has been an incredibly patient, generous soul throughout the last three years. My extended family has made valuable inputs. I am lucky to have them all.

## **Table of Contents**

### **Chapter 1**

<b>Introduction</b>	<b>8</b>
1.1 Background	8
1.2 Fracture Interactions	15
1.3 Thesis Outline	17

### **Chapter 2**

<b>Methodology</b>	<b>18</b>
2.1 Finite Element Mesh	18
2.2 PyLith	20
2.3 Benchmarks	20
2.4 Boundary Conditions	23

### **Chapter 3**

<b>Interacting Fractures</b>	<b>24</b>
3.1 A single fracture in a linear elastic solid	24
3.2 Several fractures	25
3.2.1 Effect of fracture separation	29
3.2.2 Range of influence of a single fracture in an array	32
3.2.3 Non parallel or coplanar geometries	34
3.2.4 Impact of area of the fractures	39
3.2.5 Impact of the depth of the fractures	41

### **Chapter 4**

<b>Solids with Many Interacting Fractures</b>	<b>43</b>
4.1 Fracture density	47
4.2 Poroelastic properties of the representative volume	51
4.3 Shielding vs. amplifying effects	53
4.4 Representative Volume	55

**Chapter 5**

<b>Conclusion</b>	<b>58</b>
5.1 Future work	60
<b>Appendix</b>	<b>61</b>
<b>References</b>	<b>63</b>

# **Chapter 1**

## **Introduction**

### **1.1 Background**

It is crucial to interrogate the mechanical behavior of reservoirs in order to understand the ongoing processes in their interiors. This is true for every kind of reservoir, including oil and gas, hydrological, and geothermal reservoirs. Integral to this understanding is a rigorous reservoir-monitoring regime, which allows for updated reservoir models as time progresses and the reservoir matures. During production in a reservoir, there are fluid movements and pressure changes that affect important rock properties, which can invalidate several assumptions made in a model. In order to maximize well productivity, it is necessary to utilize reservoir monitoring, which in conjunction with production data, can be used to amend shifting parameters in a reservoir model. This allows geophysicists to understand the behavior of a reservoir with time, and then gives the ability to accurately, and continually measure, analyze and predict the reservoir conditions such as pressure and production rates. This is fundamental to the overall production optimization process for any kind of reservoir.

There are several geophysical reservoir-monitoring techniques that have been used successfully, including time lapse gravimetric (Eiken et al., 2004), electromagnetic (Black and Zhdanov, 2010), geodetic (Vasco et al, 2008), and seismic monitoring (Lumley, 2001). Geodetic monitoring is a relatively new tool that has recently made significant improvements. Satellite-based geodetic techniques, in particular the Global Positioning System (GPS) and Interferometric Synthetic Aperture Radar (InSAR), have seen marked improvements in the quality of their observations, and in many cases can provide long term, cost effective monitoring. Processes taking place in an active reservoir, such as injection or withdrawal of fluid, can cause reservoir deformation, for example volume change. This deformation induces displacements within the surrounding medium. In some cases, this produces a measurable deformation at the Earth's surface. Geodetic monitoring of crustal deformation in the area overlying an active reservoir can therefore provide a powerful tool for interrogating the reservoir structure and processes.

One recent example of geodetic monitoring of an active reservoir is in the InSalah CO<sub>2</sub> storage project, at the Krechba gas fields. These fields are located in the town of InSalah, Algeria. This project involves applying carbon capture and storage (CCS) at the Krechba fields. Excess CO<sub>2</sub> from the natural gas extracted from three adjoining gas fields is gathered and reinjected into a saline formation at 1800 to 1900m depth. The CO<sub>2</sub> injection target is a 20m thick sandstone formation. This reservoir has an overburden comprised of mudstones and sandstones, which acts as a barrier to flow. While the CO<sub>2</sub> injection was ongoing, InSAR observations of the overlying ground surface were gathered. InSAR is a radar technique that uses differences in the phase of the waves reflecting off of the Earth's surface and returning to the source satellite. Maps of surface deformation can be generated using InSAR. In this way, the deformation over the active reservoir in Krechba could be determined. Over time, the ground motion induced by the injected CO<sub>2</sub> was delineated.

A study was conducted which analyzed the InSAR data associated with the injection of CO<sub>2</sub> (Vasco et al, 2008). Two satellite tracks traversed the region of deformation during the CO<sub>2</sub> injection, and the results are seen in figure 1.1. The two sets of images were interpolated to give distinct figures of the range velocity estimates over time. Figure 1.2 shows the range changes at different times. From this figure it appears that there are two lobes of range displacement decrease. This may represent uplift due to reservoir pressure changes. The largest range change overlays the injection well trace. The two-lobed pattern is evident after 96 days of injection and forms a horseshoe pattern. This pattern is suggestive of the opening of a tensile fracture at depth, and the existence of such a fracture is supported by seismic data. This feature is thought to be a vertical, or near vertical fracture, lying between the two lobes. There are therefore thought to be two major driving forces behind the surface deformation pattern. The aperture change of an extended tensile fracture, and volume change within the 20m thick reservoir. Figure 1.3 is a schematic showing the influence of pressure change in a reservoir on surface deformation. Figure 1.4 shows the influence of a tensile fracture at depth on the surface change. Figure 1.5 shows the fractional volume change within the InSalah reservoir layer, as well as the aperture change along the fracture.

It is likely that more than one fracture exists in the subsurface, and fracture interaction may complicate the stress fields in the subsurface. For example, neighboring fractures may force one another to open or close depending on the orientation. The stress fields of these fractures depends closely on the magnitude of fracture opening, and so changes in this parameter can impact any possible deformation that would be induced. The goal of this thesis is to use numerical modeling to determine the possible effects on the surface deformation when there are several interacting fractures. This is done by creating finite element models with embedded fractures and finding the additional surface displacement that would be due to these fractures. This number would then be divided by the sum of the surface displacement caused by each individual fracture. When this ratio is greater than 1, the effect of the fracture interactions is to increase the fracture openings; when the ratio is less than 1, the effect of the interactions is to decrease the fracture openings. This is termed the normalized surface displacement. The models that are used have varying numbers of fractures, with the importance of orientations, areas, and depths of fractures to be determined.

If there are appreciable interaction effects caused by the fractures in the rock surrounding the mode 1 fracture being modeled, then there are changes to the elastic moduli in the fractured media. Creating models with multiple fractures, while accounting for these interaction effects is a complicated problem; however, it may be possible to represent this fractured volume of rock with a representative volume comprised of intact rock with elastic properties that take these interactions into account. Another goal of this paper is to investigate the necessary modulus changes required to represent interacting fractures in many different fracture configurations.

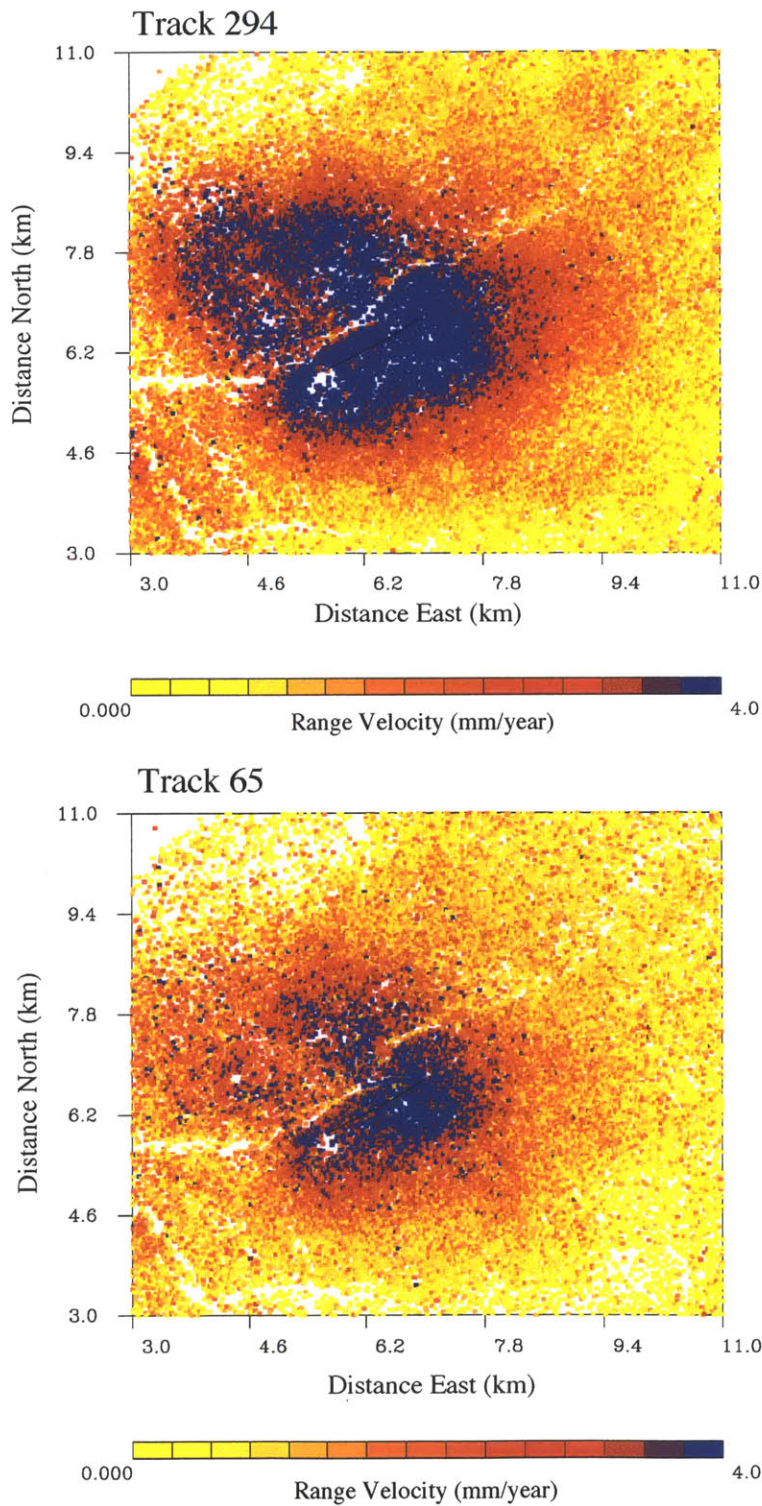


**Figure 1.1:** Two different satellite tracks showing the range velocity associated with  $\text{CO}_2$  injection at a single well. (Vasco et al, 2010)

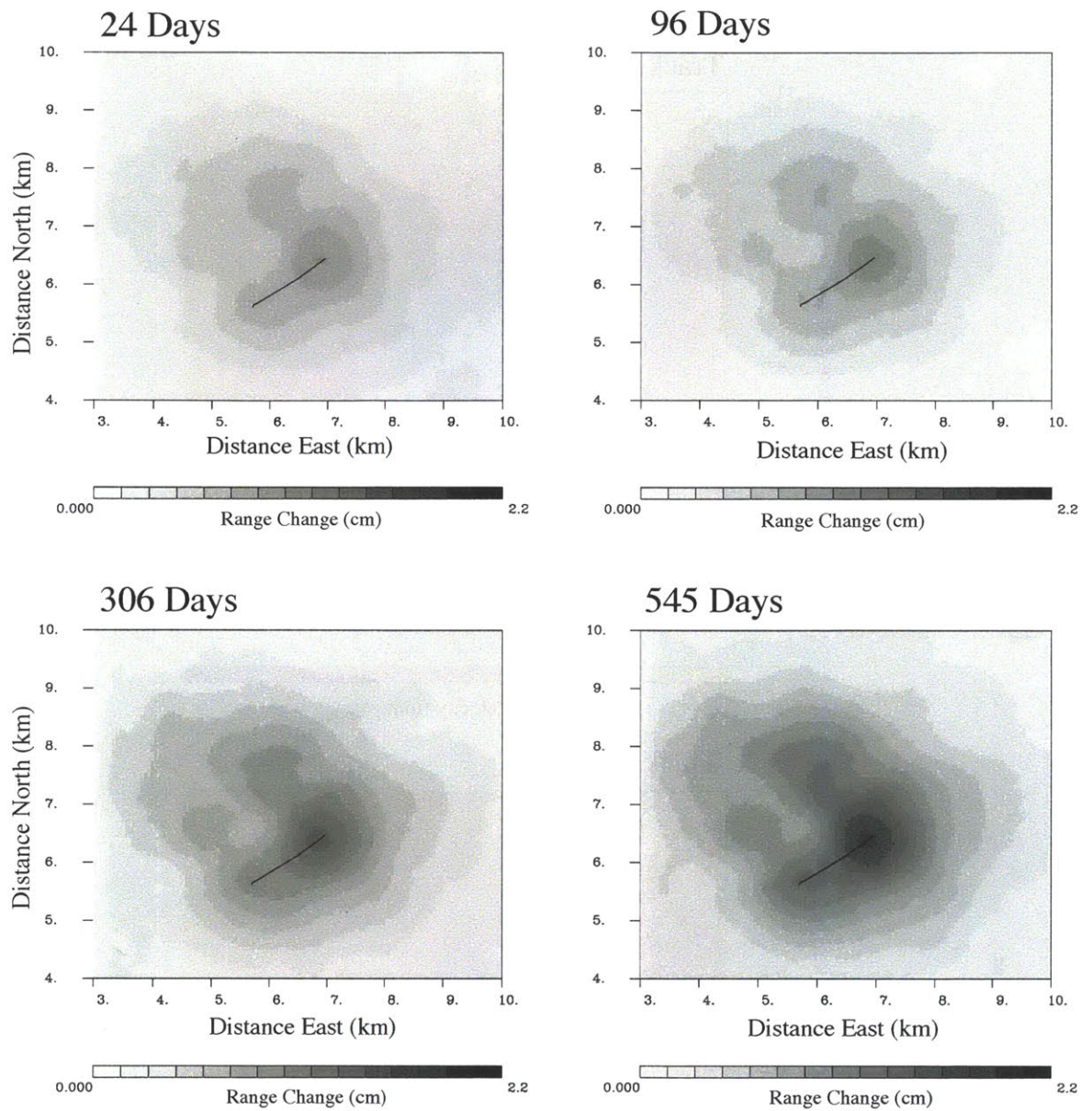


**Figure 1.2:** Range changes over time (Vasco et al, 2010)

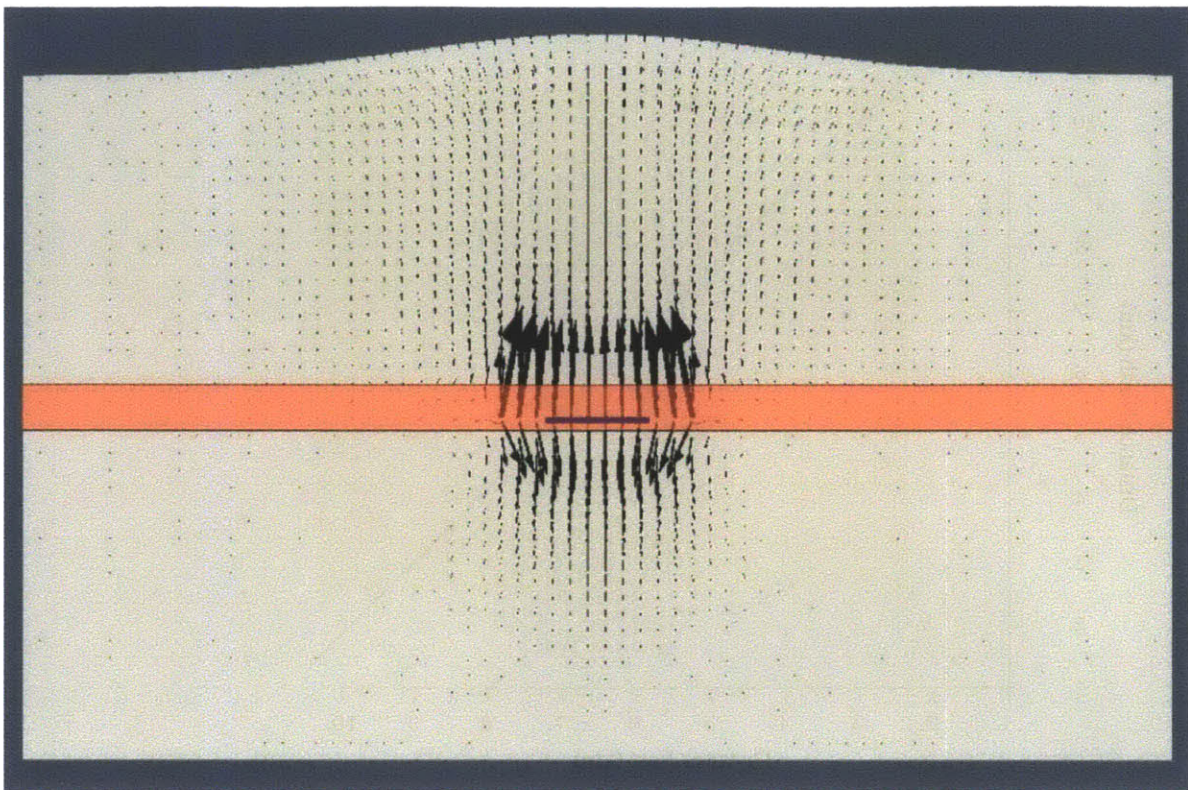


**Figure 1.3:** A vertical cross section showing how increasing pressure in the reservoir layer can cause surface deformation. The red layer is the reservoir, and the location of fluid injection is shown in purple. The arrows show the deformation in and around the reservoir. This calculation was done using PyLith, and visualized using Paraview.

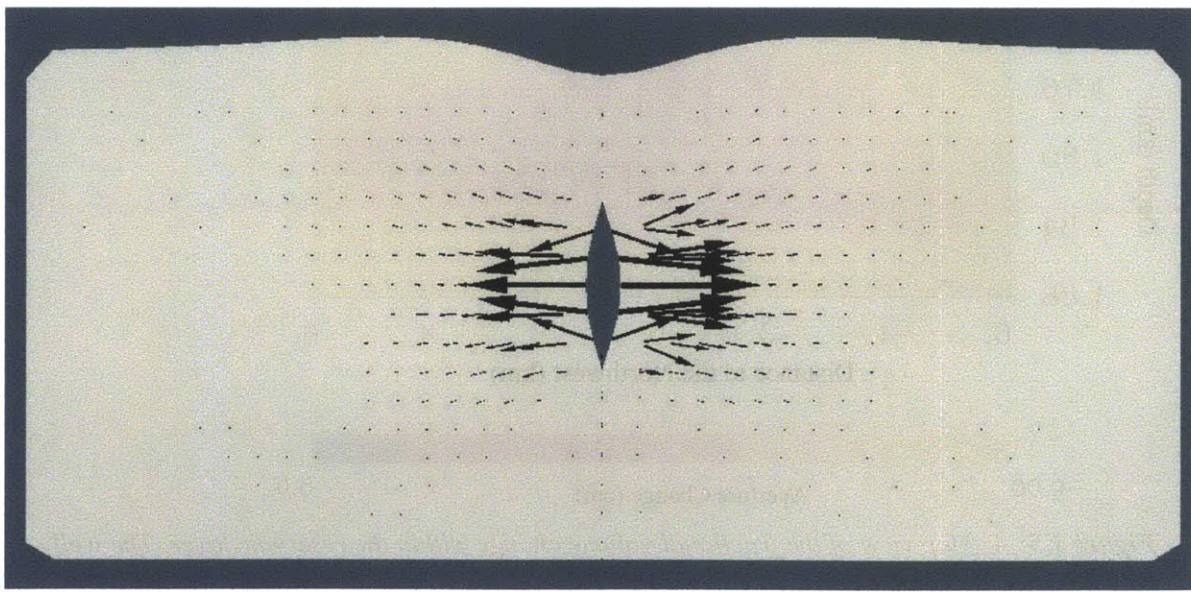


**Figure 1.4:** A vertical cross section showing how a vertical mode I fracture can cause surface deformation. The arrows show the deformation around the fracture. This calculation was done using PyLith, and visualized using Paraview.

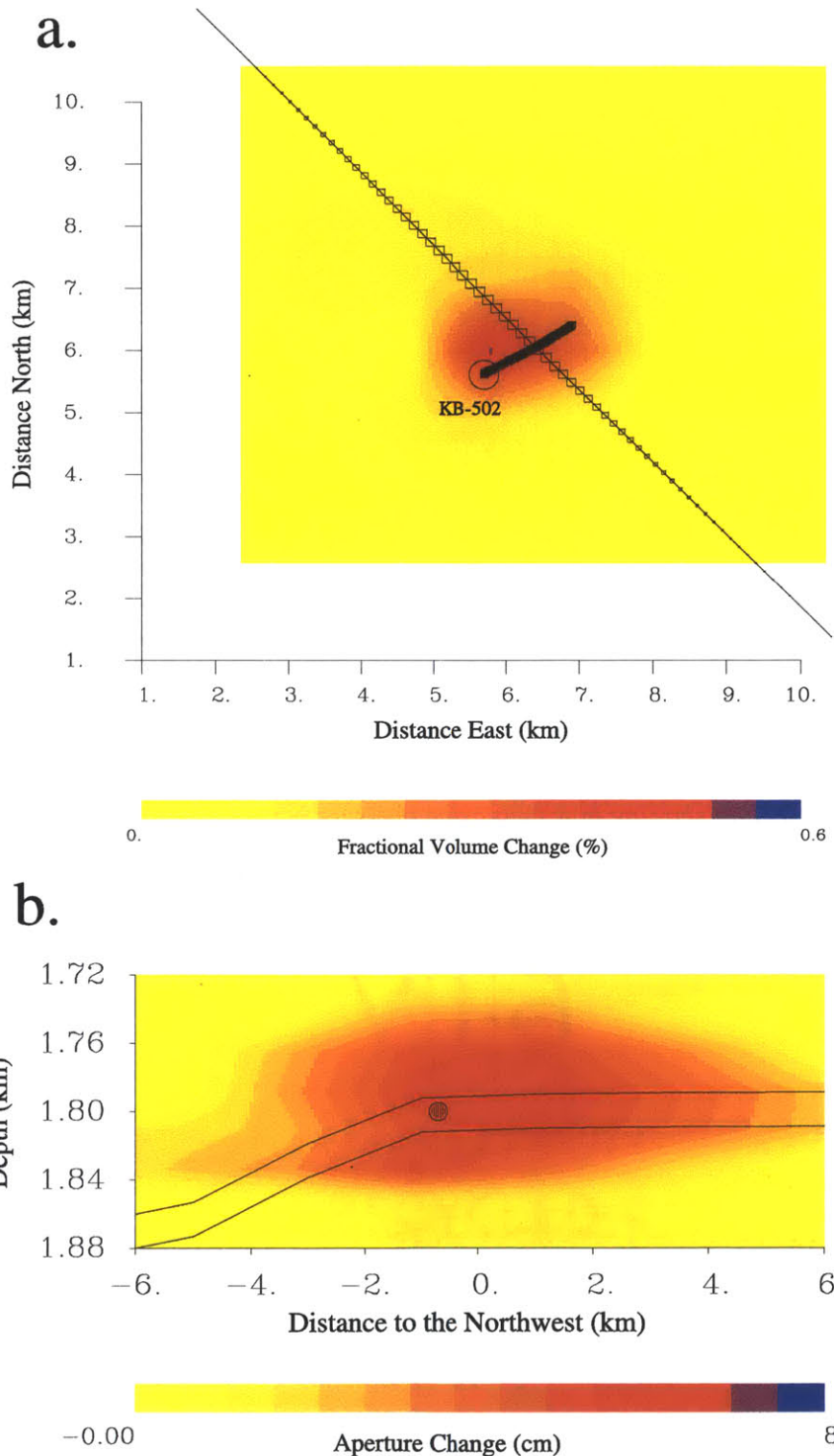


**Figure 1.5:** A: Map view of the fractional volume change within the reservoir layer. The well location (KB-502) is marked with a circle and a solid line. The northwest line represents the fracture location, while the open rectangles represent the average aperture change.

B: The spatial distribution of aperture changes over the vertical fracture; the parallel lines indicate the reservoir boundaries. The filled circle indicates the intersection of the well with the fracture plane. (Vasco et al 2010)

## 1.2 Fracture interactions

The focus of this study is to extend existing models to address the effects of several interacting fractures. This is done in two parts, each involving a different approach. The first is to examine the impact of interactions on individual fractures. This will form the bulk of this thesis. These solutions are sensitive to the position of each crack. The second part is to examine the effective elastic properties of solids with many cracks. This deals with volume average quantities, which are relatively insensitive to the positions of individual cracks. The effects of different fracture interactions on the effective elastic modulus of the surrounding rock are determined. The importance of fracture density will be considered, and then the importance of the different parameters that influence the fracture density will be examined. Additionally, the effects of these fracture parameters on the effective elastic modulus are also determined.

Finite element modeling is used to consider the manner in which interaction among multiple fractures affects surface deformation. Here these effects are investigated using a small-scale model with several dilating fractures. The response of interacting and non-interacting fractures is then compared. The effects of fracture separation, fracture size, and other aspects of the geometry and arrangement of the fractures can then be found.

While there are very good approximations for non-interacting cracks that are applicable for randomly located cracks, the cracks that are considered for this project are non-random because they are meant to simulate fractures formed in a reservoir by tectonic processes that are by nature non-random. Finding the effective moduli for a body with interacting cracks involves finding the probability distribution of the crack properties, and averaging over the orientations, positions and sizes of cracks and incorporating these to create a crack density tensor (Kachanov, 1993); therefore, in the first part of this project, these effects are examined for individual fractures. The effect of the orientation of the fractures is found by finding the difference between two representative geometries: the coplanar arrangement which has all the fractures in a single plane, and a parallel arrangement which has all the fractures in a stacked arrangement with the faces of the fractures parallel to one another.

Previous work has been done on the interaction of cracks and the elastic properties of cracked solids. These include a critical review of the effective elastic properties of cracked solids by Kachanov (1992), which he followed up with a review of elastic solids with many cracks and related problems (1994). Horii and Nemat-Nasser reviewed elastic fields of interacting inhomogeneities (1985). Nemat-Nasser reviewed the effective moduli of an elastic body containing periodically distributed voids (1981). The stiffness reduction of cracked solids (Aboudi, 1987) dealt with the problem from the point of view of engineering fracture mechanics.

Unlike these previous works, this thesis looks at the problem using finite element modeling of multiple fractures. These finite element models are created using PyLith, a 3-D finite element code. PyLith is designed to simulate crustal deformation over a wide range of temporal scales (Aagaard et al., 2007; Williams et al., 2005). The focus of this work is to determine the effect on surface deformation of fracture interactions, and this is done by comparing the mechanical response of different fracture models, some with fracture interactions, and some without.

Another goal of this work is to replace fractured media with intact representative volumes with elastic parameters that take the effects of interaction into account. This involves extending the data on the interaction of fractures to an effective continuum. The mechanical reaction of this representative volume of rock would be the same as that of the fractured rock. This would provide insight into a possible way of updating existing models to account for fracture interactions.

### **1.3 Thesis Outline**

In Chapter 2 of this thesis, we discuss the methods used to find the effects on the surface displacements, and on the stress fields of individual fractures, due to fracture interactions, using the finite element code, PyLith. In Chapter 3 we present the stress field changes and the surface displacement changes caused by fracture interactions and determine the effects of various fracture parameters. In Chapter 4 we extend the results of the fracture interactions on individual cracks to a continuum. The impact of representative volumes, which would replace fractured media, is considered. In Chapter 5 we summarize our findings and suggest future work that can be done to find the effective elastic properties of a solid with interacting fractures.

## **Chapter 2**

### **Methodology**

To investigate the impact of fracture interactions, realistic numerical models must be created that approximate the real properties of the InSalah reservoir. The numerical models that were used are finite element models which were created using Cubit, a finite element meshing software. The models were run using PyLith, a 3-D finite element code (Aagaard et al, 2007; Williams et al, 2005). The PyLith models were first benchmarked against analytical solutions in order to verify the validity of this approach. Then more complex models were built with multiple fractures.

#### **2.1 Finite Element Mesh**

The mesh is created using Cubit. The models that were used in chapter 3 used the 4-layer structure of the Rutqvist paper (2010) and their material properties. Within these models were embedded fractures that intersected the reservoir layer. There were many models built, with different fracture orientations and geometries. Figure 2.1 shows a vertical cross-section of a model with two closely spaced parallel fractures.

The material properties are taken from Rutqvist (2010). These models have fractures embedded into them in varying configurations in order to determine the effect of fracture interaction. The total surface deformation that is caused by those interacting fractures is determined by integrating the magnitude of uplift at the surface of each model. Then, these values are compared with those of non-interacting fractures, which are estimated as the sum of the deformation caused by individual isolated fractures.

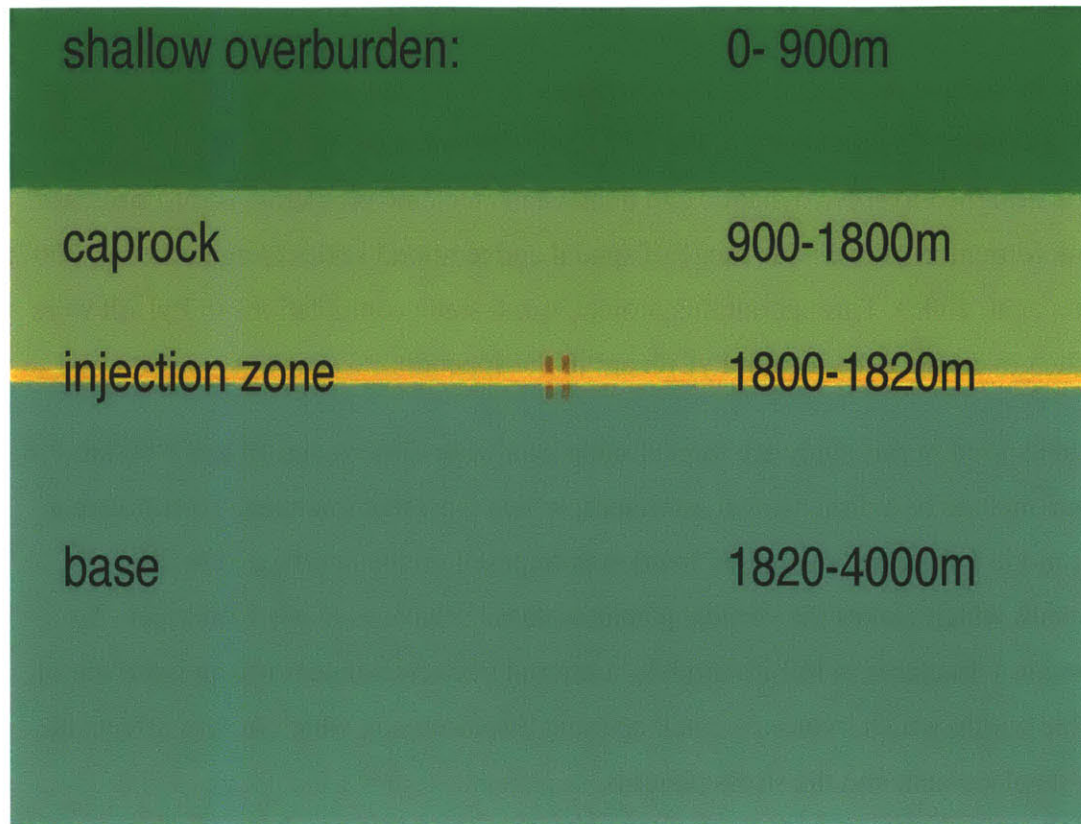


**Figure 2.1:** Vertical cross-section of a model created using Cubit

Layer	Shallow Overburden (0-900)	Caprock (900-1800m)	Injection Zone (1800-1820m)	Base (Below 1820m)
Young's Modulus, (GPa)	1.5	20	6	20
Poisson's Ratio	0.2	0.15	0.2	0.15
Effective porosity	0.1	0.01	0.17	0.01

**Table 2.1:** Material properties used in the modeling CO<sub>2</sub> injection at In Salah (Rutqvist, 2010)

## 2.2 PyLith

To compute surface displacements and variations in stress and strain, the finite element method was used. To implement it, the 3-D finite element code: PyLith, is utilized. PyLith is designed to solve dynamic and quasi-static tectonic problems, and to simulate crustal deformation over a wide range of spatial and temporal scales (Aagaard et al, 2007; Williams et al, 2005). Throughout this project, quasi-static computations in PyLith were used. The governing equations in PyLith are in the appendix.

The models used in this study are three dimensional with dimensions  $10\text{ km} \times 10\text{ km} \times 4\text{ km}$ . They include two-dimensional interfaces, which represent fractures. To simulate a dilating mode 1 fracture, an applied traction is imposed on the interface. The stress is extensional, which makes the vertical planar surfaces behave as mode 1 fractures. To create mode 1 fractures in PyLith models, a normal traction is input onto an interface of negligible width, which induces a crack opening displacement, which in turn affects the surface displacement and the stress patterns.

## 2.3 Benchmarks

To verify the validity of the approach, the solutions from PyLith must be benchmarked against the analytical solutions from Okada. To do this, the differences in the two solution methods must be rationalized. The analytical solution was found via Coulomb, a deformation and stress-change boundary element software, which use the Okada analytical solution (Toda et al., 2005; Lin, Stein, 2004). A crack opening displacement of 0.25m was input onto a rectilinear fracture of dimensions 800m \* 800m at 2000m depth. The PyLith models created to compare solutions are composed of a homogeneous material. The tractions to be imparted onto the fracture interface were found using the relation between the average crack opening displacement and the tractions required to induce this displacement (Kachanov, 1992)

$$\langle b_n \rangle = \frac{16(1-\nu^2)n}{3\pi E} \sqrt[3]{\frac{2A^2}{\pi P}} \quad (2.1)$$

where  $b$  is the crack opening displacement due to a normal force,  $n$ ,  $A$  is the area and  $P$  is the perimeter of a non-circular crack.  $\nu$  is the Poisson's ratio,  $E$  is Young's modulus.

Crack opening is constant in the analytical model, while in the PyLith model the opening of the mode 1 fracture is not constant. This is because applied tractions are used for the PyLith models and this gives rise to a natural fracture opening solution, which is not constant over the face of the fracture, but the Okada analytical solutions only apply for a constant fracture displacement. The value of  $b$  is prescribed in the analytical solution, and Coulomb is used to find the displacement boundary conditions for the PyLith model. With these boundary conditions, the PyLith model is run with the constant tractions found from equation 2.1.

Even though there are differences between the models used to create the analytical and PyLith solutions, they still give rise to an acceptable benchmark comparison. Saint-Venant's principle states that the difference between the effects of two different but statistically equivalent loads becomes very small at sufficiently large distances from the load. The domain of both models is much larger than the fracture length. With the boundary conditions, the domain can be seen as even larger. As the models have statistically equivalent loads acting upon fractures with equal dimensions, we can use Saint-Venant's principle to argue that the benchmark comparison is acceptable.

To benchmark the PyLith solutions against the Okada analytical solutions, the surface displacements in the X, Y and Z directions were compared. These are seen in figure 2.2. The normalized root mean square error for the PyLith solution is 1.33 % in the X direction, 2.98% in the Y direction and 4.04 % in the Z direction. These results are for a mesh resolution of 100m x 100m x 100m, in the 8000m x 8000m x 4000m block. The results improve as the grid spacing decreases from 500m to 100m. The effect of the grid size on the normalized RMSE is shown in figure 2.3.

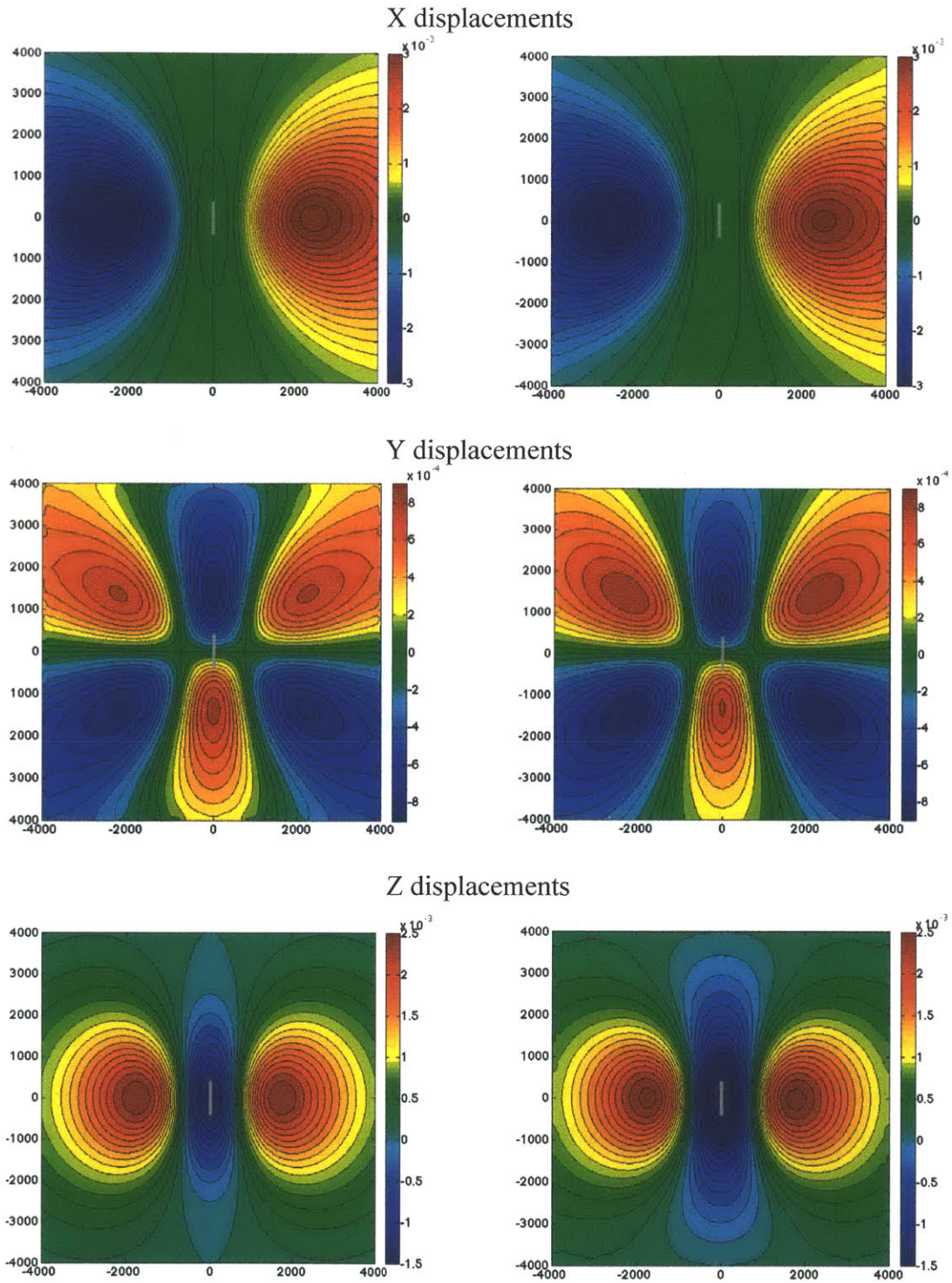


**Figure 2.2:** Surface displacements for a single mode 1 fracture in an elastic medium. X, Y and Z displacements where X is positive to the right, Y is positive in the up direction and positive Z goes out of the figure. The gray lines in the center of each image represent the location of the fracture. Analytical solutions are on the left, solutions from PyLith on the right.

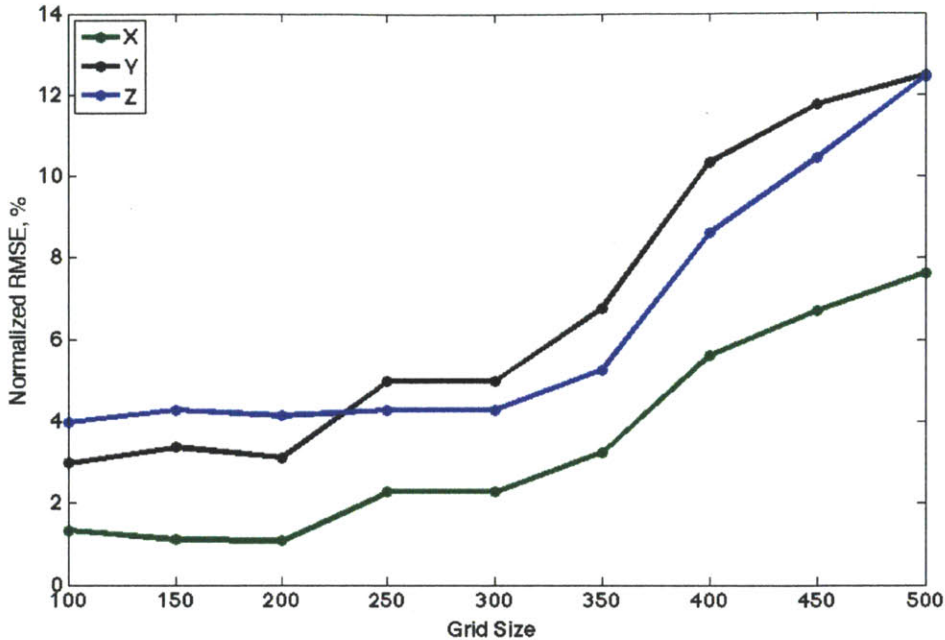


**Figure 2.3:** A plot of the normalized RMSE vs. the grid size.

## 2.4 Boundary Conditions

Edge effects can be very significant as the models are of a finite domain; therefore the boundary conditions are calculated using Coulomb. The solutions from Coulomb are for an elastic half-space with uniform isotropic elastic properties, while models made in PyLith are made in a block of finite dimensions. The displacements in the Coulomb solution at the locations that would constitute the boundary of the block used in the PyLith simulation are found, and then input onto the boundary of the PyLith model as Dirichlet boundary conditions to rationalize the difference between the finite blocks of PyLith and the half-space of the analytical solution. This is done for the benchmarks, which need to be as accurate as possible. In the case of interacting fractures, this is not a feasible solution because the analytical solution does not take interactions into account. To get around that problem roller boundary conditions are put into place, which allow no displacement in the X or Y directions at the sides, and no displacement in the Z direction at the base of the domain. For a domain as large as the one used for these models, these are reasonable boundary conditions.

## **Chapter 3**

### **Interacting Fractures**

#### **3.1 A Single Fracture in a Linear Elastic Solid**

In order to examine the mutual interactions of fractures, the effect of a single fracture must first be considered. Consequently, the stress fields generated by a single fracture in a linear elastic solid are the starting points for this study. The mode 1 stress fields are examined for a single fracture and the results determined in Pylith are compared with the analytical solutions from Okada (1985). The analytical solution from Coulomb and the numerical solution from Pylith for the normal stress perpendicular to mode 1 field are seen in figure 3.1.

The normal stress can be seen to radiate outwards in two regions, normal to the fracture and along the plane of the fracture. In the region normal to the fracture, the stress is negative and therefore compressive. This region is larger than the positive, tensile region of stress along the plane of the fracture. The large compressive area is a shielding zone, and in interactions with other fractures has a shielding effect. The range of this effect is larger than the amplifying effect created in the tensile region of the stress field. The shielding and amplifying effects on nearby cracks can therefore be predicted by the geometry. If a fracture is in the shielding zone of another fracture, it should have a lower magnitude stress and surface deformation than it would otherwise, but if it were in the amplification zone, the magnitude of these properties should increase.

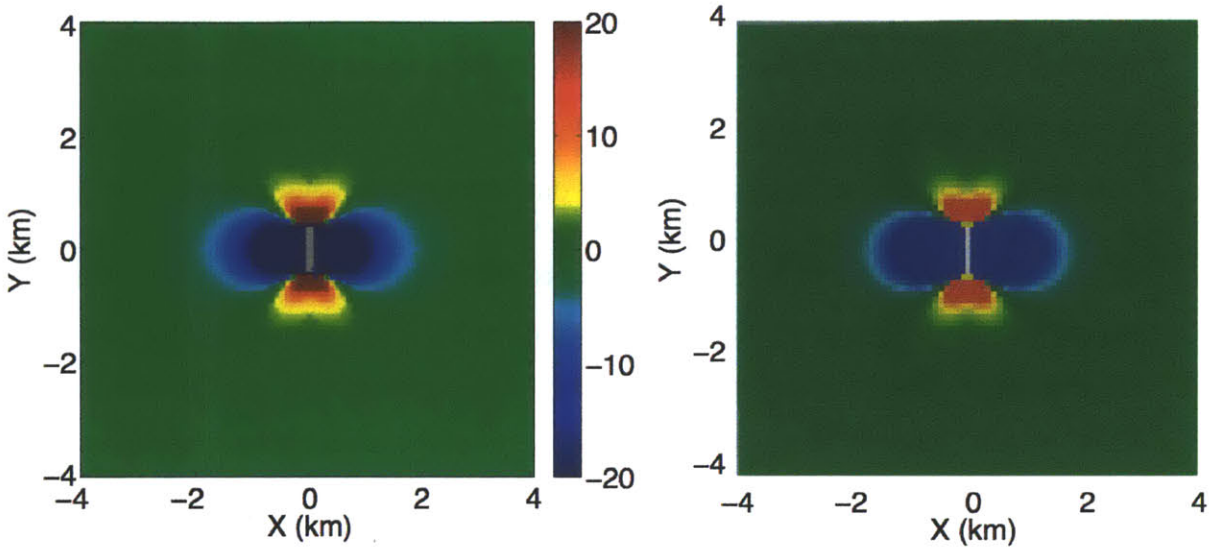


**Figure 3.1:** Stress fields for the normal stress generated by a mode I fracture in map view over a horizontal cross section of the model. On the left are the Okada analytical results for the stress field; on the right are the results from Pylith. The grey lines in the center of each image represent the fracture location. The color scale is the same for both, normal stress change in bars, unclamping positive.

### 3.2 Several Fractures

Now that the stress fields and surface displacements resulting from a single fracture in an isotropic linear elastic solid have been modeled, the method can be extended to the problems involving several cracks. As before, there is an infinite linear elastic solid with tractions prescribed at infinity, but now there are several traction free cracks. To model the stress interactions, we use the same basic model that was used to investigate the single crack, with the same boundary conditions; but in this case there are several fractures added.

The problem of tractions at infinity influencing several cracks can be replaced by the equivalent problem: crack faces loaded by tractions with stresses vanishing at infinity. The traction on the  $i$ th crack is represented as:

$$t^i = n^i \cdot \sigma^0 + \sum_{j \neq i} \Delta t^{ji} \quad (3.1)$$

where  $n^i$  is the unit normal to the crack face,  $\sigma^0$  is the stress on the crack face, and  $\Delta t^{ji}$  is the traction generated onto the  $i$ th crack by the  $j$ th crack which itself is loaded by traction  $t$  (Kachanov, 1993). This shows that the total stress on the crack is the sum of the initial loading ( $n^i \cdot \sigma^0$ ) and the stresses transmitted onto the crack by nearby cracks ( $\Delta t^{ji}$ ).

To get an understanding of the additional stress, the total surface deformation is found by integrating the total vertical uplift caused by the cracks. Using the fact that the surface deformation is directly related to the amount of crack opening, the ratio between the uplift caused by the interacting cracks ( $u$ ), and the uplift caused by the non-interacting cracks ( $u'$ ) is found. This ratio ( $u/u'$ ) is used as the measure of the effect of fracture interactions. Values greater than 1 correspond to stress amplification, while values less than 1 correspond to stress shielding. Whether or not there is stress amplification or stress shielding depends on the geometry. To show this, two different representative geometries are examined: the coplanar configuration in which all of the fractures are in each other's amplification zone; and the parallel configuration in which all of the fractures are shielded.

To illustrate the change in surface displacement for both coplanar and parallel geometries, models with three fractures each were created. The surface displacement along a line passing through all three fractures is found and the vertical displacements are displayed in figures 3.2 and 3.3. The displacements for interacting fractures are shown alongside those of non-interacting fractures, which are found by summing the displacements for 3 separate isolated fractures in the same locations. We can see that the surface displacement magnitude decreases for parallel fractures, and increases for coplanar fractures. We also see that the impact of interactions is clear when the fractures are proximate to one another, but for distant fractures there is little difference between the interacting and non-interacting cases. Another observation is that for parallel fractures, the change in surface displacement is larger than for coplanar fractures.

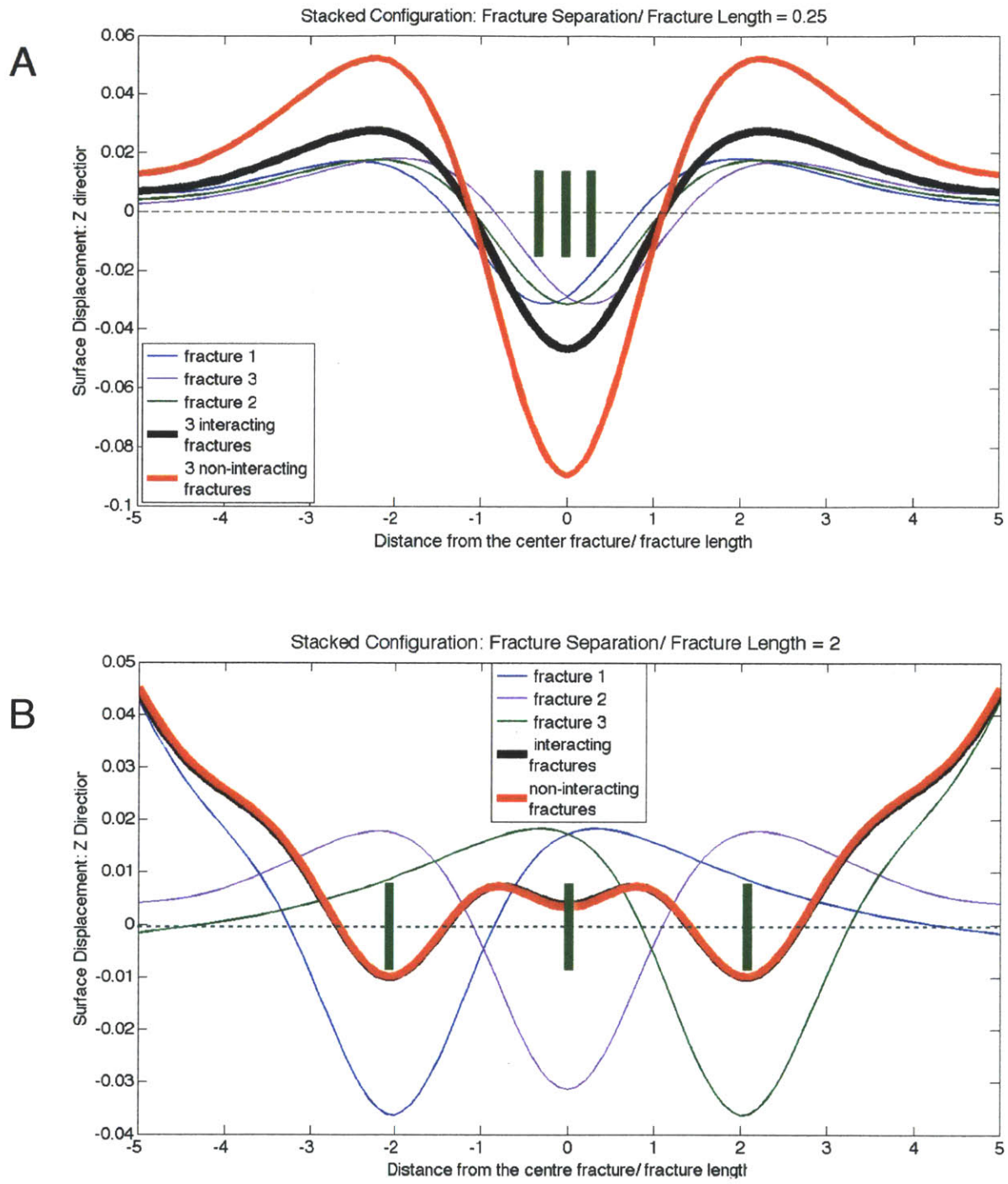


**Figure 3.2:** The vertical surface displacement along a line through all 3 fractures in a parallel configuration. (A) The fracture separation is  $0.25 \times$  the length of the fracture. (B) The fracture separation is  $2 \times$  the length of the fracture. The fracture locations relative to one another are shown in green.

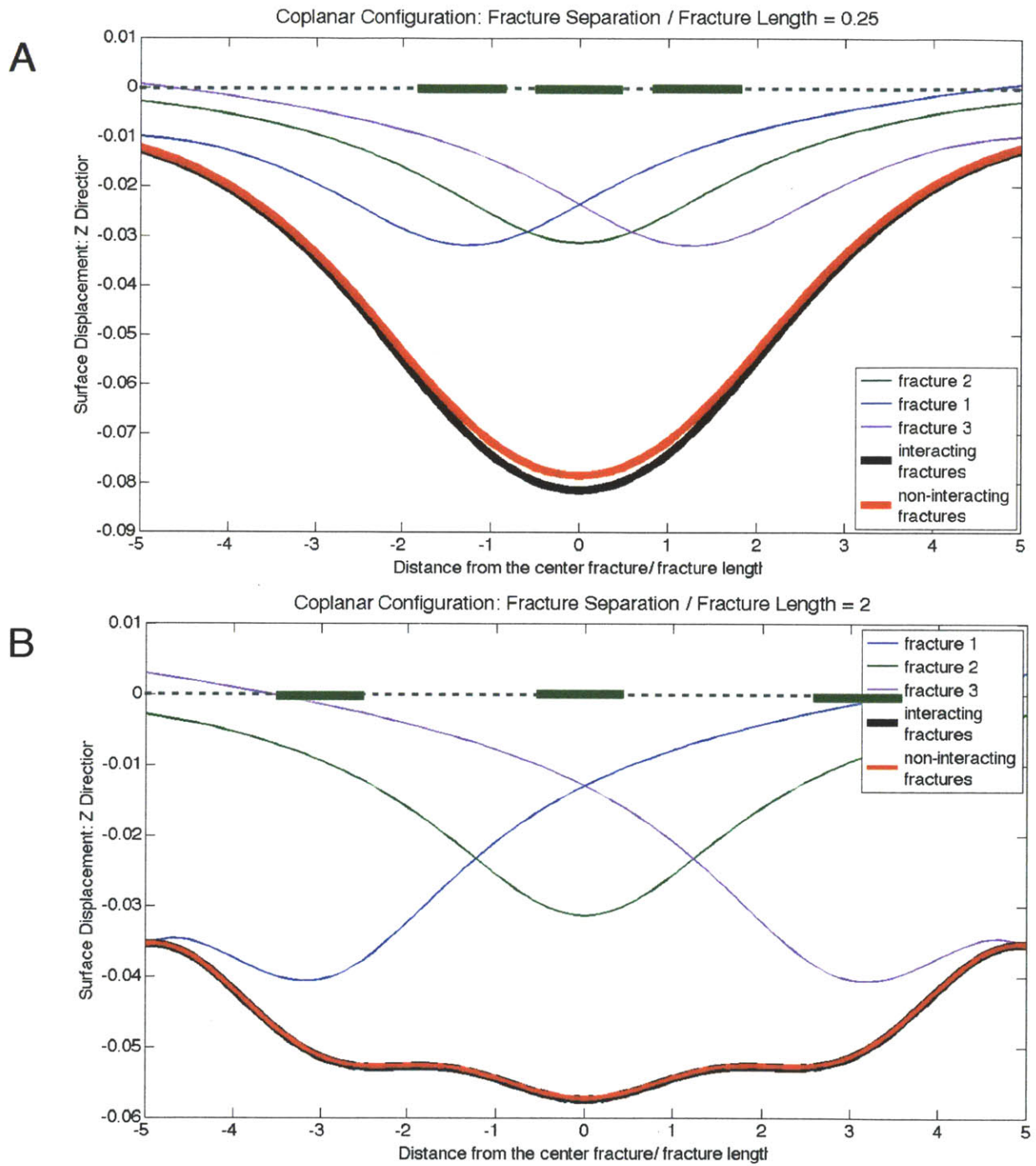


**Figure 3.3:** The vertical surface displacement along a line through all 3 fractures in a coplanar configuration. The fracture separation is 2 x the length of the fracture. The fracture locations relative to one another are shown in green.

### **3.2.1 Effect of Fracture Separation**

The separation between the tips of neighboring fractures is a major determinative factor in the magnitude of fracture interaction. To illustrate this, models with two fractures, in the coplanar and parallel geometries, are created with varying fracture separations. The change in the  $u^i/u^o$  ratio as fracture separation increases is shown in figure 3.4, for both the coplanar and parallel geometries. These results are consistent with figures 3.2 and 3.3, as the smaller the fracture separation, the larger the change in the surface deformation,  $u^i/u^o$ . It is also clear that the impact of interactions is wider for stress shielding than for stress amplification, as the magnitude and extent of the interaction effect is larger in the parallel geometry, than in the coplanar geometry. For the coplanar geometry, the fracture interactions always increase the magnitude of surface deformation, while for the parallel geometry the fracture interactions always decrease the overall surface deformation.

To illustrate the extent to which the shielding effect dominates over the amplifying effect, models containing four fractures in double parallel configuration are created. In this case there is competition between the amplifying and shielding effects, and the overall change in fracture opening depends on the relative distance between the fractures. The separation between the parallel and coplanar fractures was varied and figure 3.5 shows the results of this competition.

The effect of shielding has a larger magnitude and a larger range and so the spacing between the stacked fractures must be further away than the spacing between the coplanar fractures for the stresses to balance. This corroborates the results in figure 3.4.

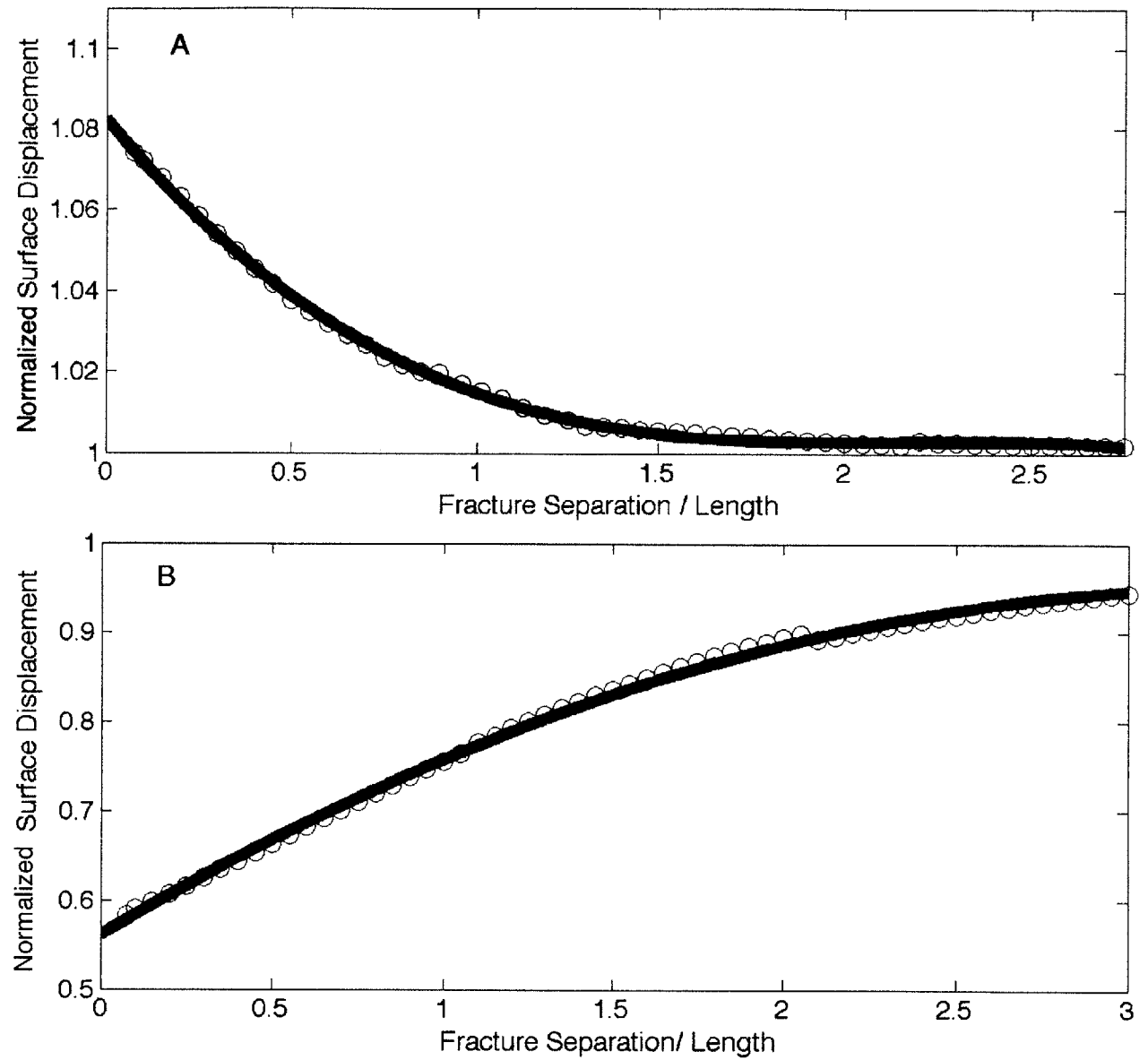


**Figure 3.4:** A: The effect of fracture separation on the ratio  $u/u^0$  in the coplanar geometry.  
 B: The effect of fracture separation on the ratio  $u/u^0$  in the parallel geometry.

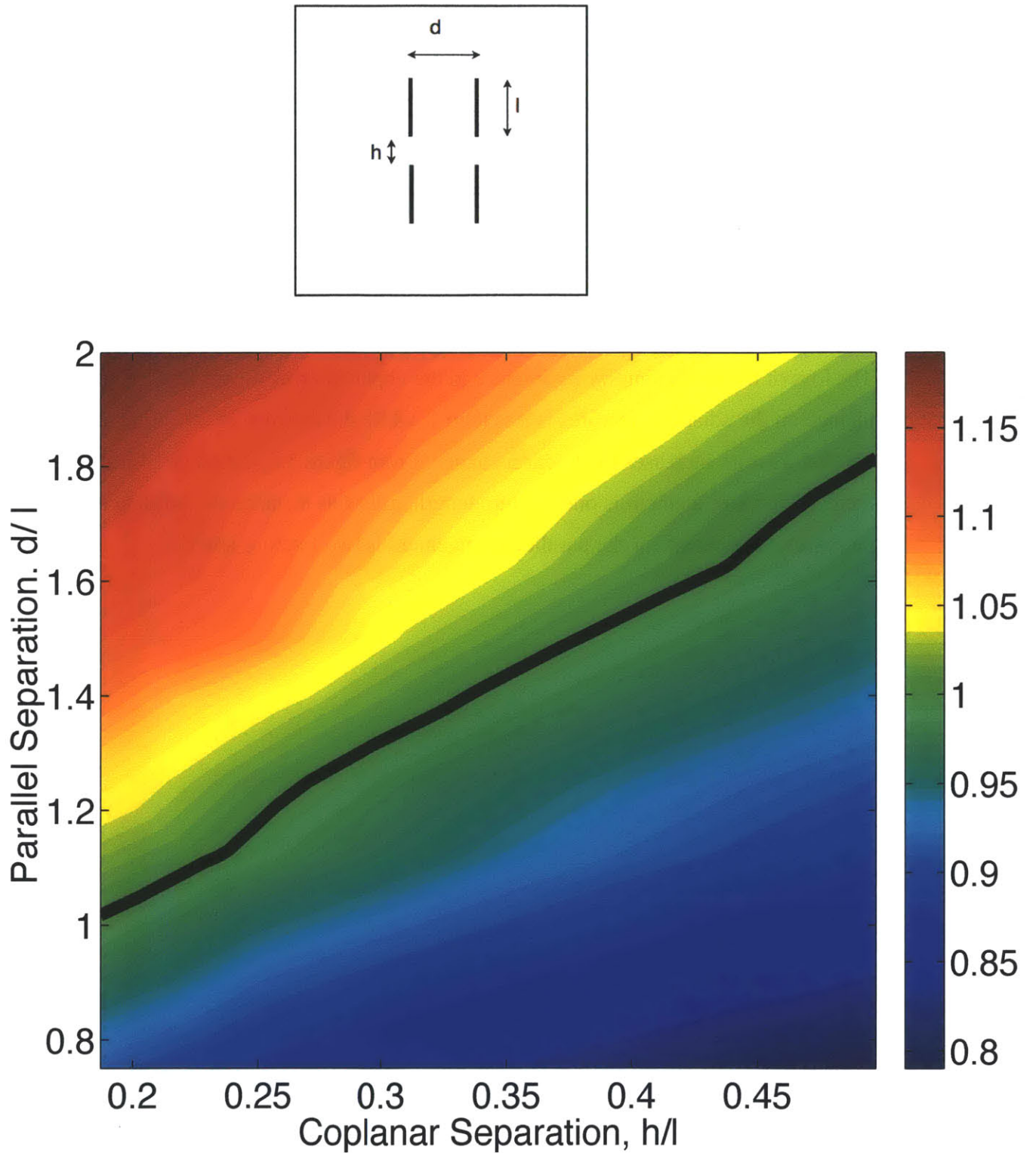


**Figure 3.5:** Competition of the amplification and shielding effects. The red region on the map is where the  $u/u^0$  ratio is greater than 1, the blue region is where it is less than 1. The model used to create this figure is seen above.

### **3.2.2 Range of Influence of a Single Fracture in an Array**

Two periodic patterns of 11 fractures are considered, a coplanar array with the space between the fracture tips at one quarter of the fracture length, and a stack of parallel cracks with the space between the fractures at one half of the crack length. A disturbance is created by removing the fracture in the center of the array. In this case, the normal tractions are loaded from the boundaries and the fractures are represented as very thin, very low modulus regions. The traction change on the adjacent fractures is shown in figure 9.

The loss of the stress amplifying fracture in the coplanar array means that the traction change on the adjacent fractures is less than 1, while the removal of the stress shielding parallel fracture increases the traction change. From figure 3.6, the range of influence in the coplanar arrangement is one fracture length, after this distance the influence is negligible. The range for the parallel arrangement is two fracture lengths.

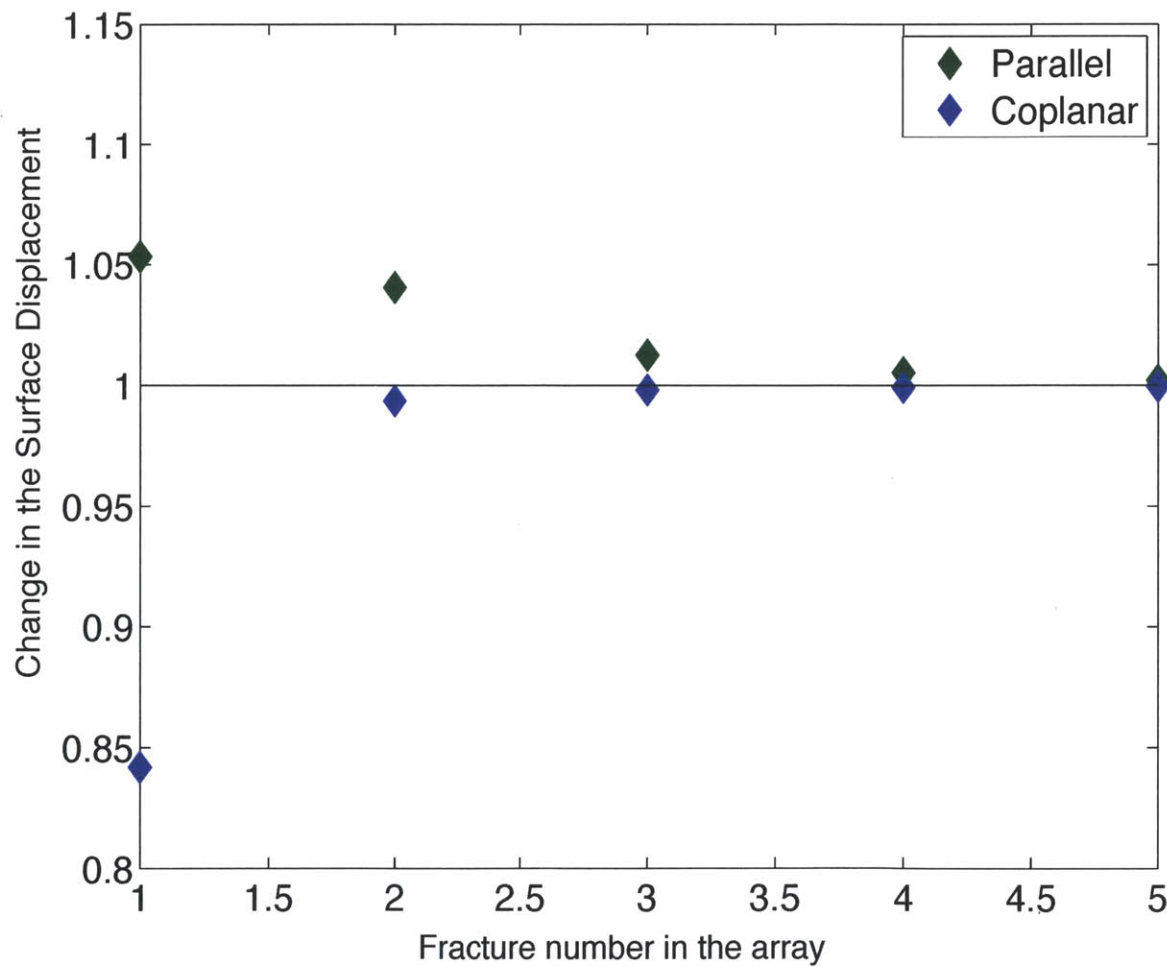
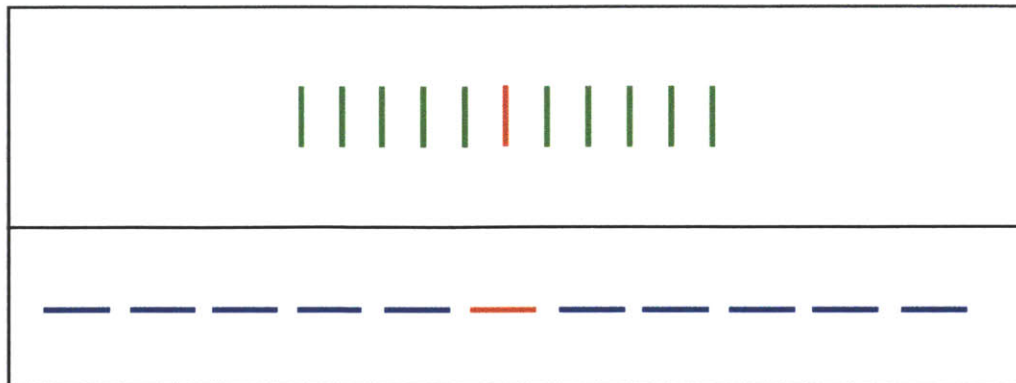


**Figure 3.6:** The range of influence of a single fracture in an array of fractures. The models used to make these figures are seen above, in mapview. In green are the parallel fractures; the red fracture in the middle is removed. In blue are the coplanar fractures; the red fracture in the middle is removed.

### 3.2.3 Non parallel or coplanar geometries

In order to expand this study, the effect on the surface displacement in asymmetric arrays is found. To examine these asymmetric arrays, the starting point is the same 2 fracture models that have been used in their coplanar and parallel geometries. This time, instead of having perfect symmetry, one of the fractures is disturbed. This gives rise to interesting effects.

The first case of disturbed symmetry was done on two parallel fractures of equal areas and depth. The fractures have a separation of 1.5 times the fracture length. One of the fractures is rotated about the vertical axis from  $0^\circ$  to  $90^\circ$ . The change in surface deformation due to fracture interactions is found as this angle changes and these results are seen in figure 3.8. The same concept is used for coplanar fractures. Beginning with two fractures in the same plane with a fracture separation of 0.25 times the fracture length, one of the fractures is rotated about the vertical axis. Again the change in the  $u^i/u^o$  ratio is found for different angles, from  $0^\circ$  to  $90^\circ$ . These results are seen in figure 3.9.

Another way to evaluate the effect of disturbed symmetry is to determine the change in surface displacement due to interacting oblique coplanar fractures. In this case, the starting point is again two coplanar fractures, but then the position of one of the two fractures is varied in the direction of its normal. These results are found in figure 3.10.

The interesting results from this section come from the coplanar fractures. The disturbance in symmetry actually gives rise to a slightly larger change in the  $u^i/u^o$  ratio. The maximum change in surface displacement does not take place at  $\phi = 0^\circ$ , but at  $\phi \approx 10^\circ$ . This occurs for both the rotated fracture and the oblique fracture. A possible reason for this is the fact that the stationary fracture in both cases is affected by both normal and shear tractions from the rotated fracture. The stress amplification due to normal traction is maximal at  $\phi = 0^\circ$ , however, the additional stress amplification due to shear tractions caused by the rotated fracture exceeds this at low angles.

This is manifest in the oblique arrangement as well. When the symmetry of the coplanar configuration is slightly disturbed by translation, the change in the surface deformation

increases. Figure 3.10 shows that the maximum normalized surface displacement occurs away from the parallel configuration, while the fractures are in each other's amplification zone, but not quite in the shielding zone. As the parallel separation increases, the shielding effect is felt, even though amplification still dominates.

Interestingly, the coplanar and parallel fractures become the same when  $\phi = 90^\circ$ . These are perpendicular fractures. The normalized surface displacement is greater than 1 for this configuration, even though the shielding effect usually dominates in this situation. This is due to the fracture geometry, and the way in which fractures close and open their neighbors. Figure 3.7 shows the deformation for perpendicular fractures. Shielding occurs when arrows normal to the plane of a fracture arrive normal to the plane of another fracture and push that fracture closed, thus reducing its aperture. Amplification occurs when contraction at the crack tip increases the amplitude of a neighboring fracture. Amplification is therefore effective regardless of the fracture geometry, while shielding is only effective in a somewhat parallel orientation.

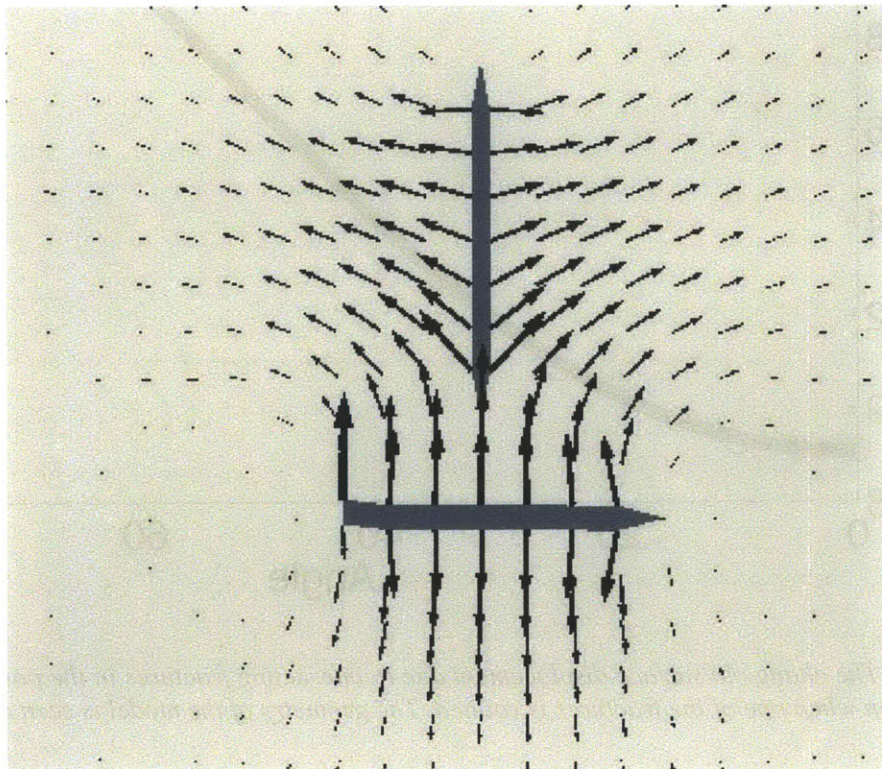


**Figure 3.7:** The deformation caused by perpendicular fractures. This calculation was done using PyLith, and visualized using Paraview.

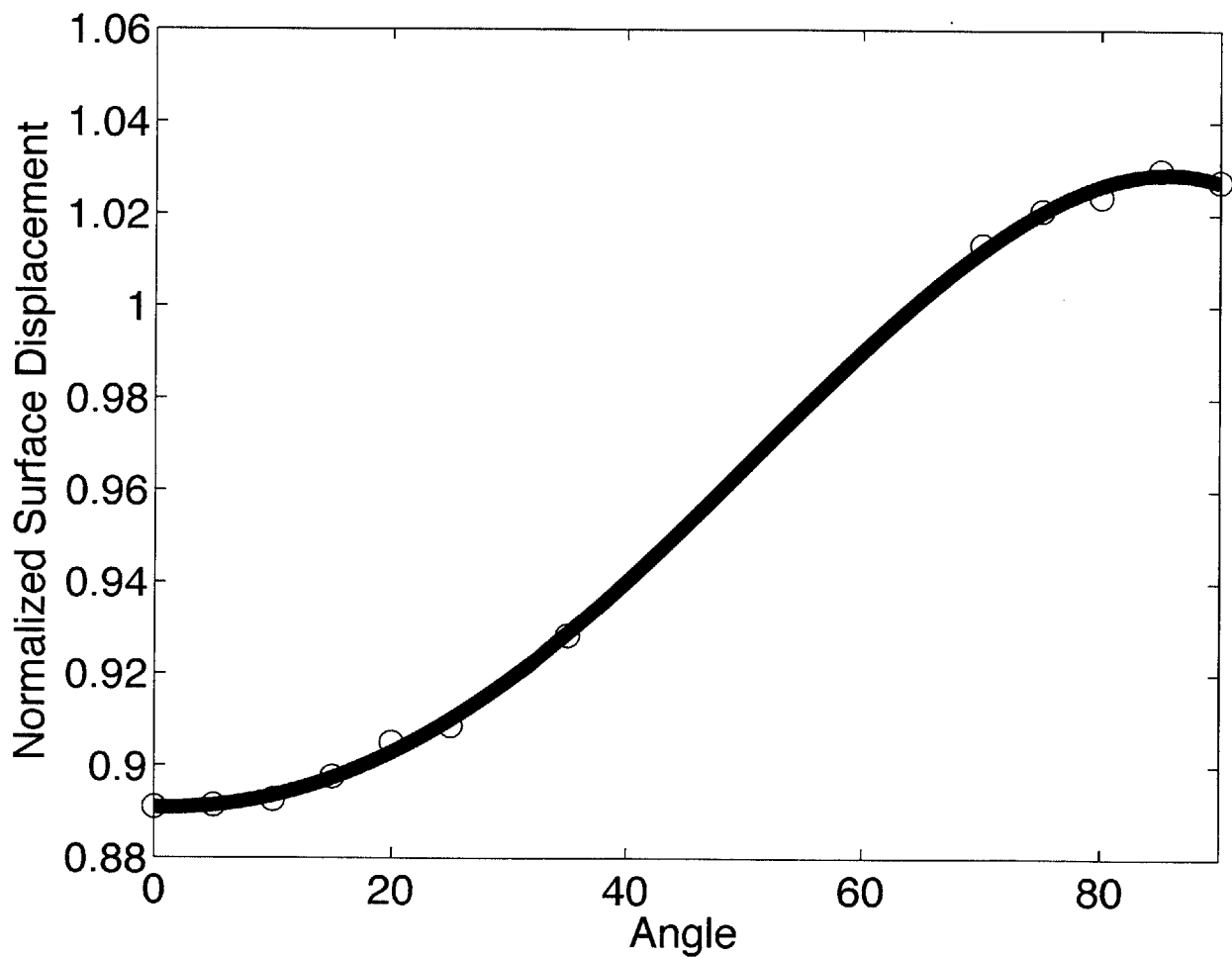
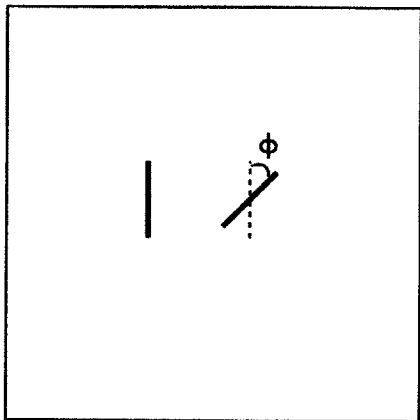


**Figure 3.8:** The change in surface displacement due to interacting fractures in the parallel configuration when one of the fractures is rotated. The geometry of the model is seen above.

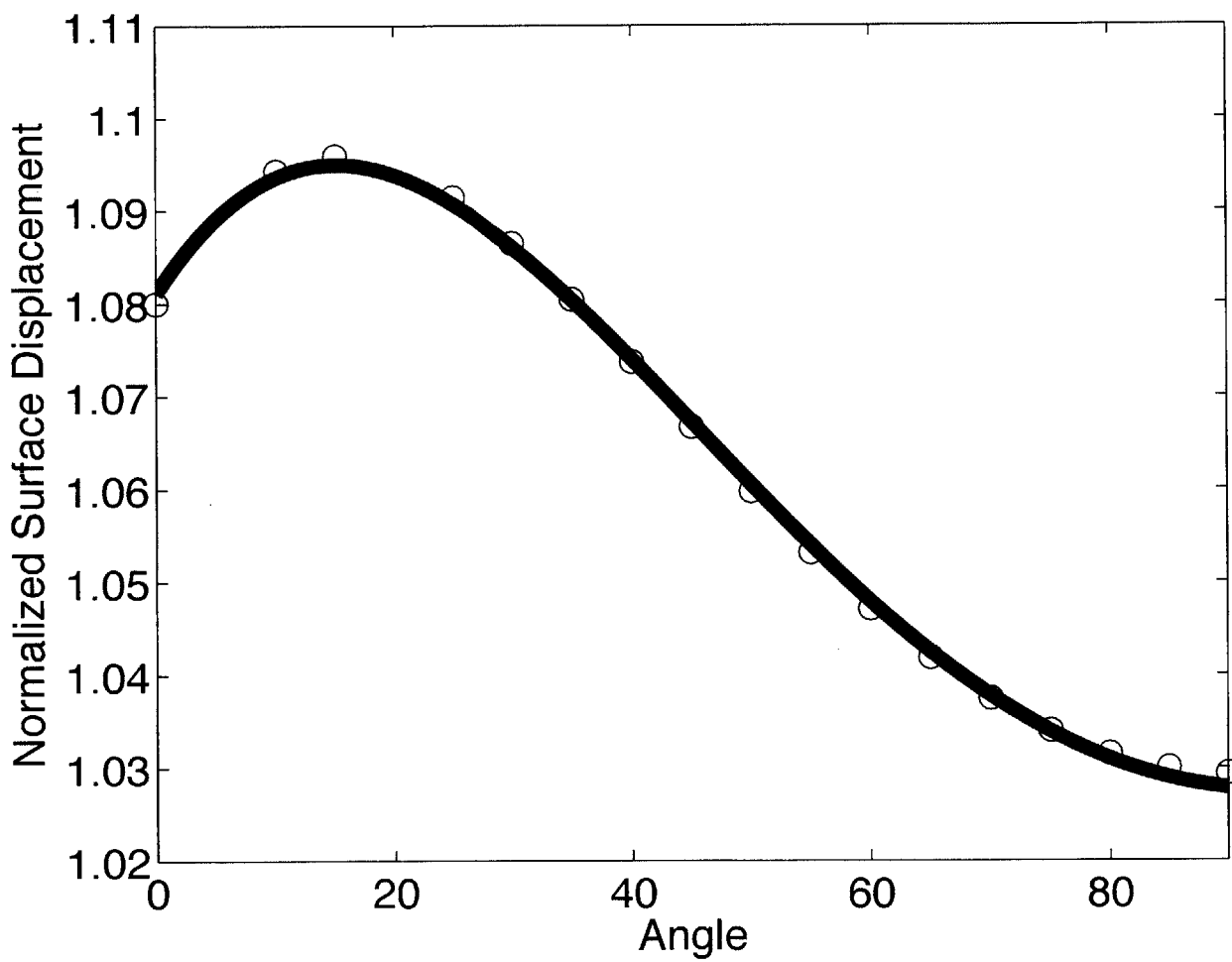
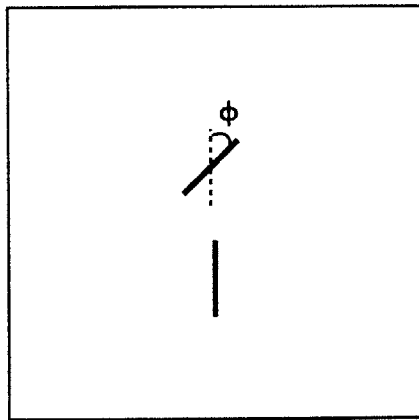


**Figure 3.9:** The change in surface displacement due to interacting fractures in the coplanar configuration when one of the fractures is rotated. The geometry of the model is seen above.

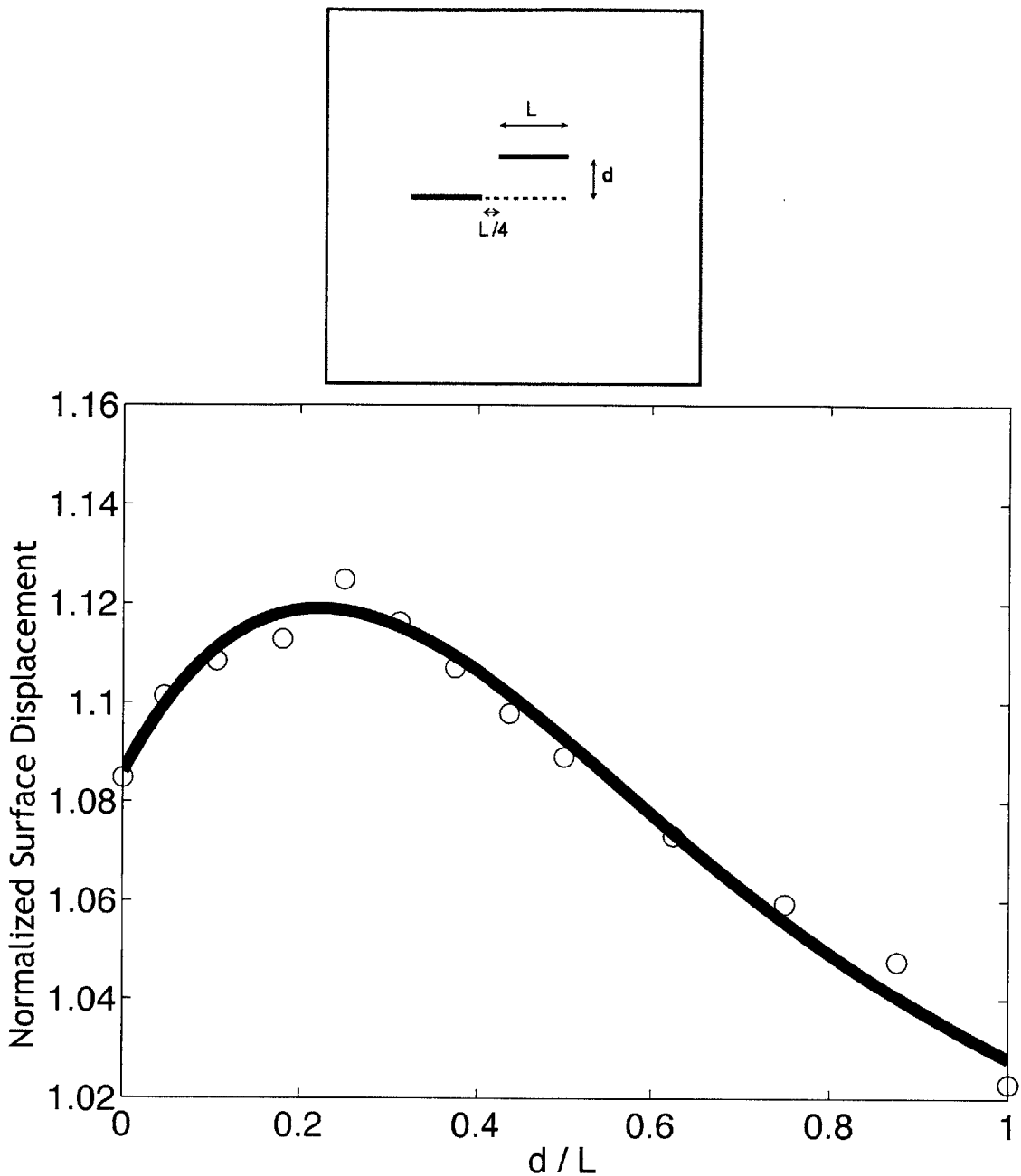


**Figure 3.10:** The change in surface displacement due to interacting fractures in the coplanar configuration with symmetry disturbed by translation. The geometry of the model is seen above.

### **3.2.4 Impact of the Area of the Fractures**

In order to determine the effect of the area of the fractures on the stress interactions, models containing two fractures of equal dimensions and depths are created in both coplanar and parallel configurations. This was done for several fracture sizes; in each model, the fracture separation was equal to the fracture length. Figure 3.11 shows the results of this exercise with the fracture interactions plotted against the area of the fractures. We can see that the normalized interaction effects actually decrease as the fracture area increases. For the coplanar configuration, the normalized surface displacement decreases as the fracture area increases, while for the parallel configuration the normalized surface displacement increases as the fracture area increases. Interestingly, these trends are reversed when the fracture separation is kept constant, instead of being kept equal to the fracture length.

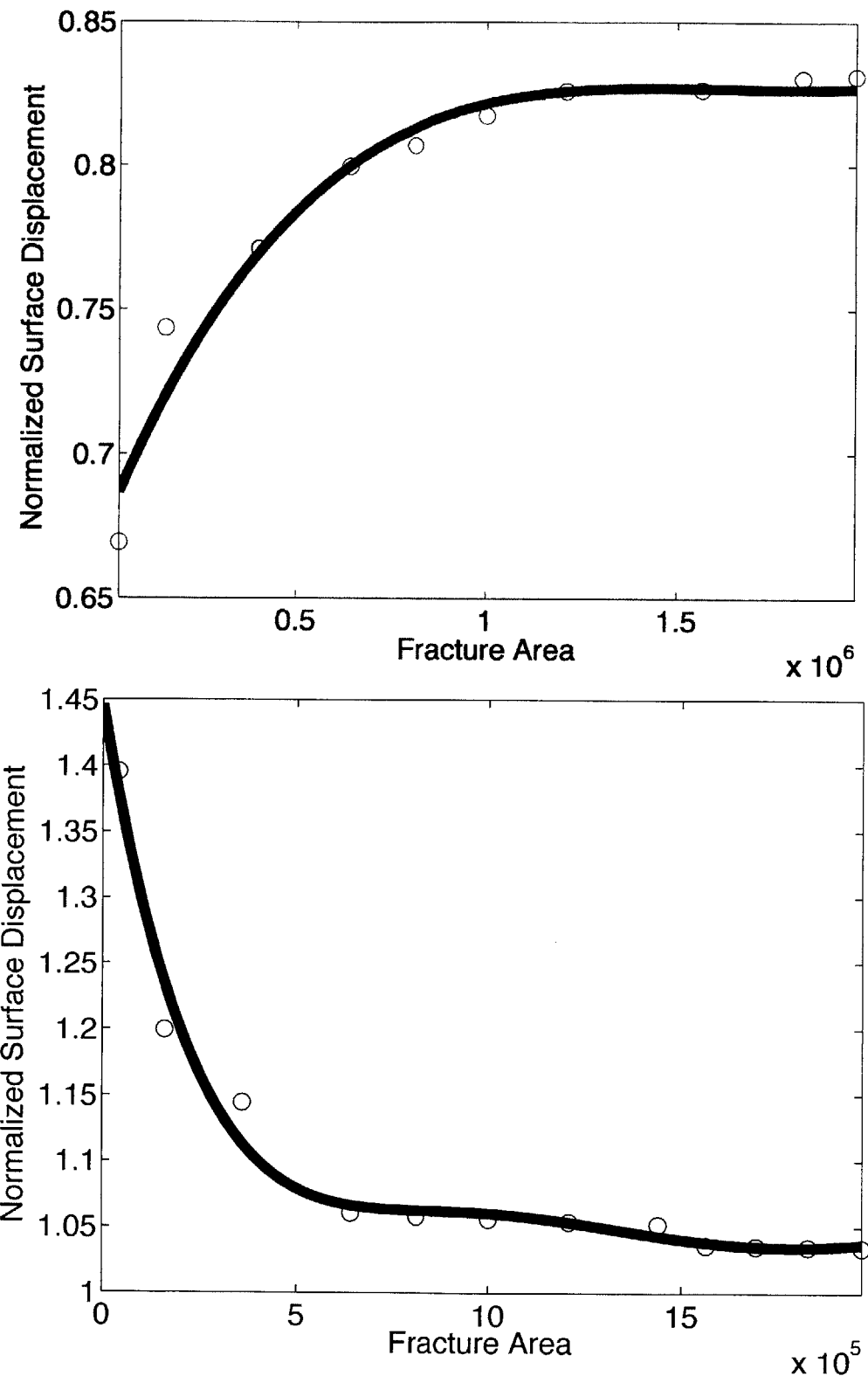


**Figure 3.11:** The effect of fracture area on the surface deformation caused by fracture interaction. Above: fractures in a parallel configuration. Below: coplanar fractures.

### **3.2.5 Impact of the Depth of the Fractures**

To determine the impact of the depth of the fractures, the magnitude of the change in the surface displacement was found using a model with three fractures, each at the same depth, in the coplanar arrangement. Each fracture had a rectilinear 800m x 800m shape, and the depths were varied from 1000m to 3000m. To find the importance of depth on the fracture interactions, the magnitude of the surface displacement generated by the model with interacting fractures was divided by the surface displacement generated when the fractures do not interact.

The results for non-interacting fractures were found by summing the displacements for three models of isolated fractures in the same locations as in the model of interacting fractures. The results show that even though the magnitude of the surface displacement decreases with depth, the effect of the fracture interactions actually increases with depth. This can be seen in figure 3.12.

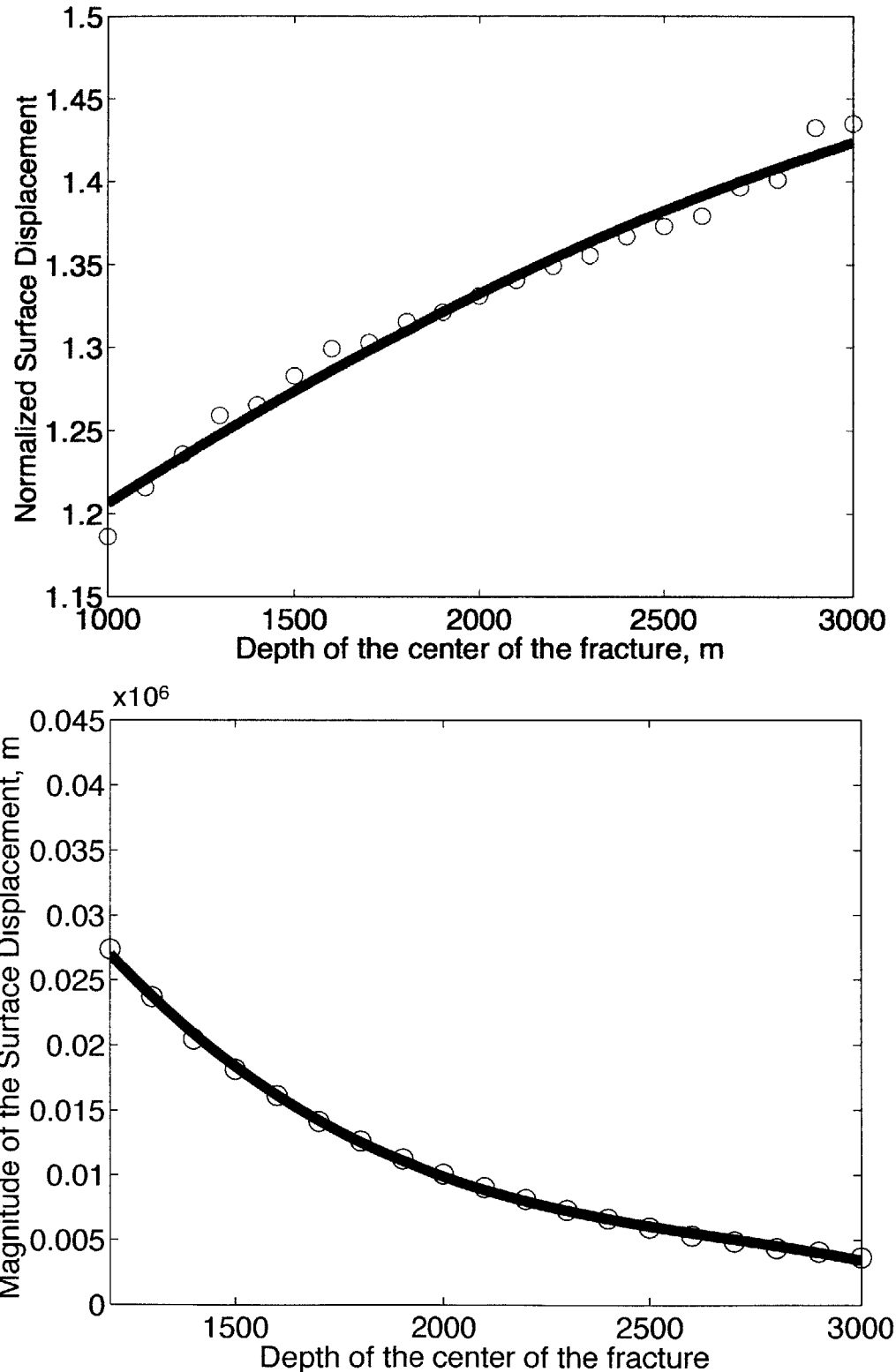


**Figure 3.12:** Above: the importance of depth in the change in the normalized surface displacement due to fracture interactions. Below: The importance of depth in the magnitude of the surface displacement.

## Chapter 4

### Solids with Many Interacting Fractures

The second part of this project is to use the information from the impact of interactions on individual cracks and extend it to find the effective elastic properties of fractured solids. These elastic properties predict reduction of stiffness, development of anisotropy and changes in wave-speed (Nemat-Nasser, 1981). The existence of fractures creates an additional compliance

$$\Delta M = \left( \frac{1}{2V} \right) \sum S^i (\hat{n} \cdot B \cdot \hat{n})^i \quad (4.1)$$

where  $\Delta M$  is the additional compliance,  $V$  is the volume,  $S$  is the area of a fracture and  $B$  is the crack opening tensor, which depends on the crack opening displacement,  $b$  (Kachanov, 1993). From this equation it is clear that the additional compliance is due to the fracture displacement and the fracture density, which is found by

$$\rho = \frac{2}{\pi} \frac{1}{V} \sum \left( \frac{S^2}{P} \right)^i \quad (4.2)$$

for a volume,  $V$ , fracture area,  $S$ , and fracture perimeter,  $P$  (O'Connell and Budiansky, 1976).

The constitutive equations for a linear poroelastic medium are:

$$2\mu \epsilon_{ij} = \sigma_{ij} - \frac{\nu}{1+\nu} \sigma_{kk} \delta_{ij} + \frac{(1-2\nu)\alpha}{1+\nu} p \delta_{ij} \quad (4.3)$$

$$\Delta m = \frac{(1-2\nu)\alpha p_0}{2\mu(1+\nu)} \left[ \sigma_{kk} + \frac{3}{B} p \right] \quad (4.4)$$

Equation 4.3 relates the strain,  $\epsilon_{ij}$ , to the stress acting on the material element,  $\sigma_{ij}$ , and the pore pressure,  $p$ . Equation 4.4 relates the change in fluid mass per unit volume,  $\Delta m$ , to the mean normal stress,  $\sigma_{kk}$ , and pore pressure, where the Biot pore-pressure coefficient,

$\alpha$ , and the Skempton coefficient,  $B$ , are constants.

When a volume of fluid is injected into a reservoir, the pore pressure increases, thus changing the strain. The existence of fractures in the reservoir increases the compliance, and at the same time decreases the pore pressure. Fluid injection into a fractured reservoir would therefore induce a lesser strain than fluid injection into an intact reservoir. The fractures themselves create an effective change in the elastic moduli of the reservoir, which decreases the expected surface deformation. The current models assume that there is a single dilating fracture in an intact volume of reservoir rock. To amend these models to account for a fractured reservoir, the region of reservoir rock containing fractures must be accounted for. In this paper, this region will be represented as an intact volume of rock with an altered Young's modulus and an altered Poisson's ratio.

To quantify the change in the material properties needed to accurately represent a region of fractured rock, a representative volume which comprises the fractured region is identified. Figure 4.1 shows the representative volume and the surrounding rock. The Young's modulus inside this representative volume is varied between 15 GPa and 50 GPa, while the Young's modulus in the surrounding region is held constant at 25 GPa. A single fracture is embedded within the representative volume and the change in the surface displacement caused by the changing Young's modulus is found. Then a new set of models is created in which the Poisson's ratio inside the representative volume is varied between 0.10 and 0.35, while the Poisson's ratio of the surrounding rock is held constant at 0.25. In this way, the effect of changing the elastic properties in the region surrounding a single fracture, which represents a fractured region, is found. Figure 4.2 shows the change of the total surface displacement when the Young's modulus is varied. Figure 4.3 shows the change of the total surface displacement when the Poisson's ratio is varied.

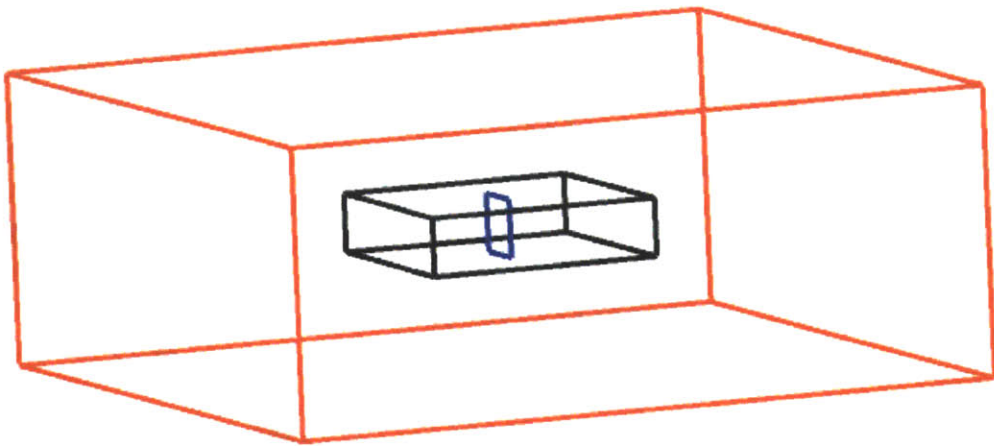


**Figure 4.1:** A sketch of the representative volume in black with the fracture in blue, surrounded by the unaltered rock in red.

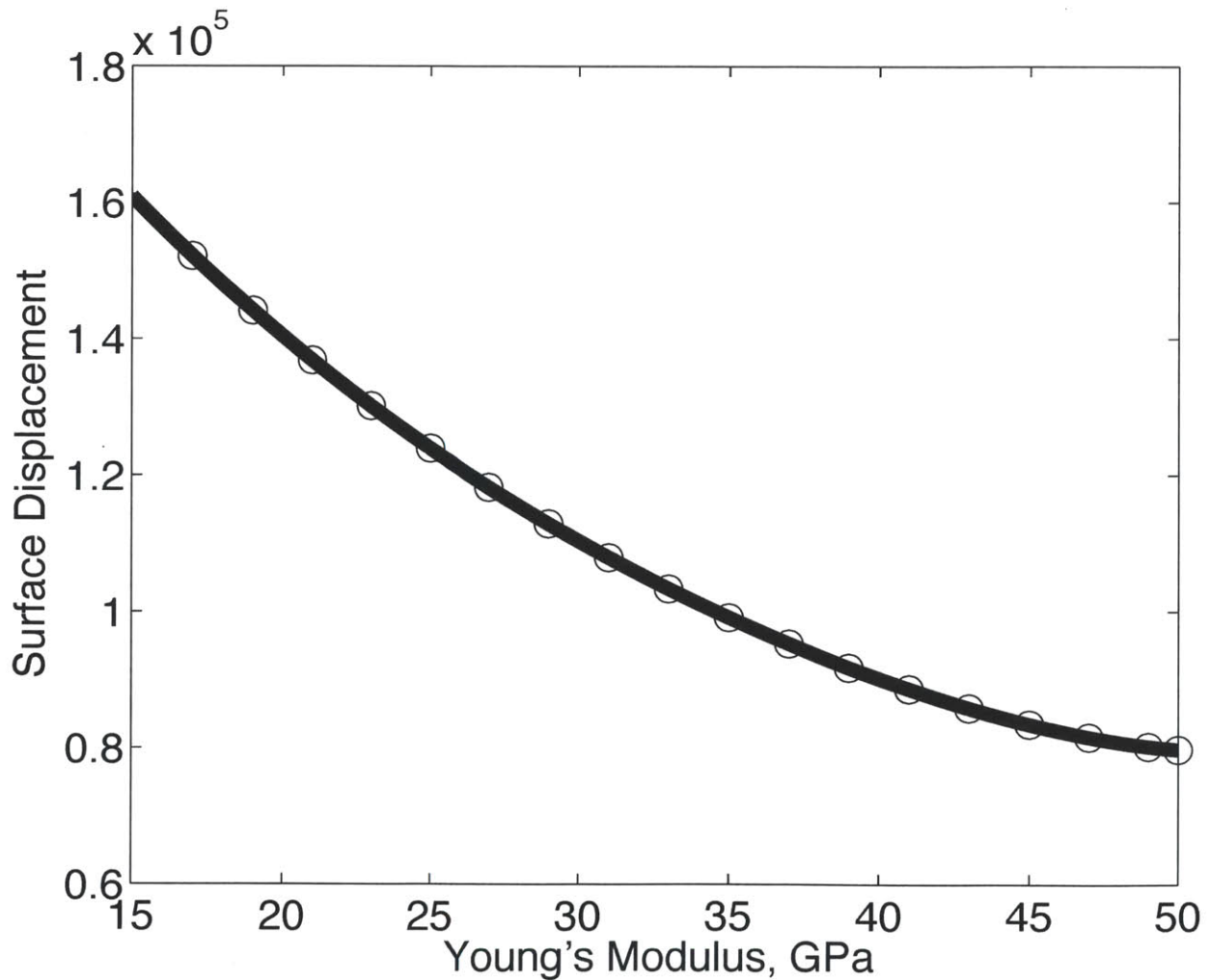


**Figure 4.2:** The change in the total surface displacement caused by a single dilating fracture in a confined region, when the Young's modulus of that region is varied.

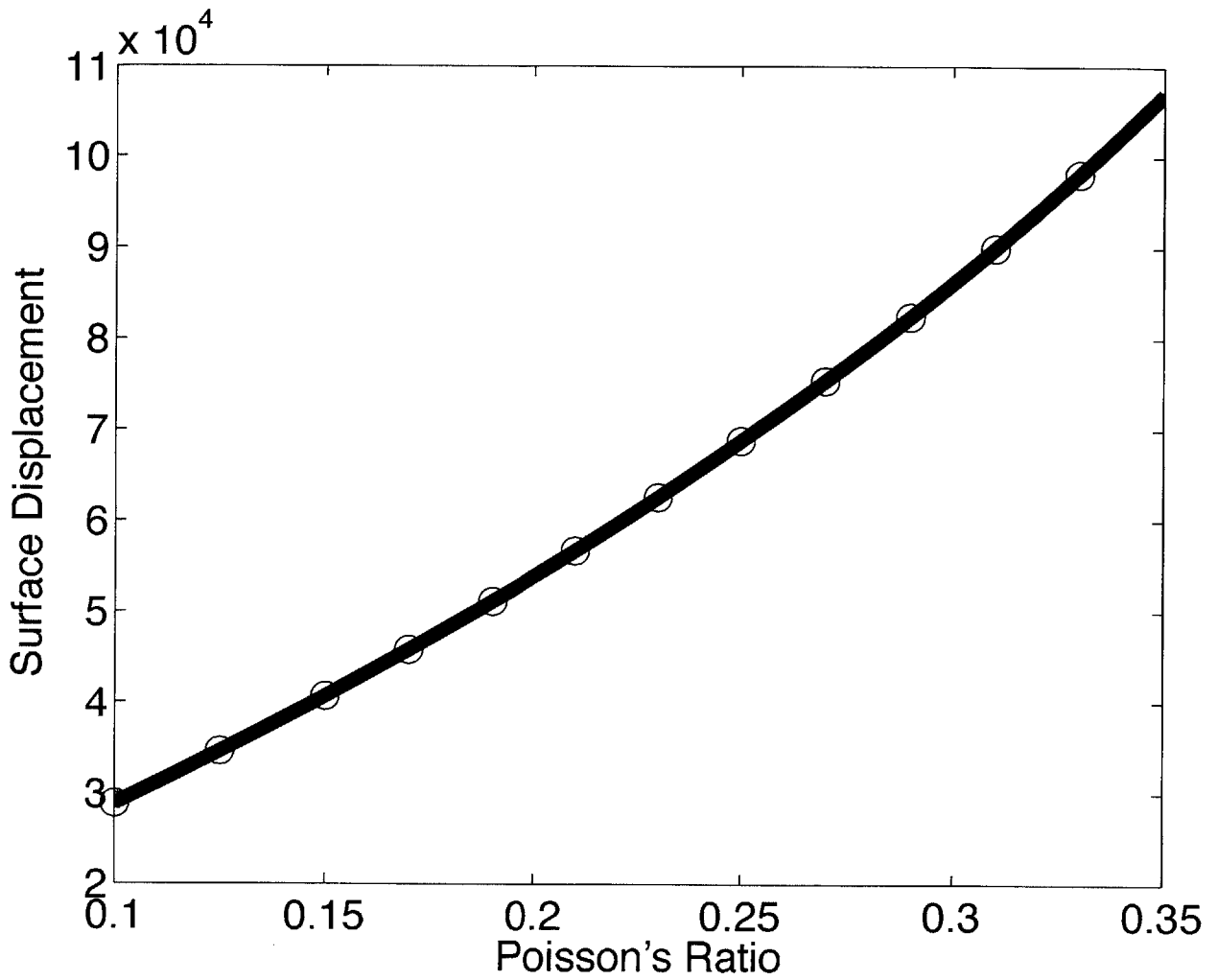


*Figure 4.3: The change in the total surface displacement caused by a single dilating fracture in a confined region, when the Poisson's Ratio of that region is varied.*

We have seen that fracture interactions can have an effect on the elastic properties and change the expected surface deformation. In addition to finding the elastic properties needed to account for the fractures themselves, the impact of the fracture interactions are found in order to fully delineate the effect of the fractured reservoir. The changes to the Young's modulus and Poisson's ratio needed to account for the fracture interactions are investigated for different fracture densities.

#### 4.1 Fracture Density

The fracture density is the most important parameter when it comes to the additional compliance. The larger the fracture density, the greater the additional compliance in the rock. To examine the fracture density, models containing 1, 4, 9, 16 and 25 fractures in a square configuration are created. The fractures are all contained in the representative volume and have the same dimensions, meaning that the fracture density is solely dependent on the number of fractures. Figure 4.4 is a colormap showing the change in total surface displacement due to the number of fractures in a representative volume with a changing Young's modulus. Figure 4.5 shows the surface displacement when the Poisson's ratio is varied.

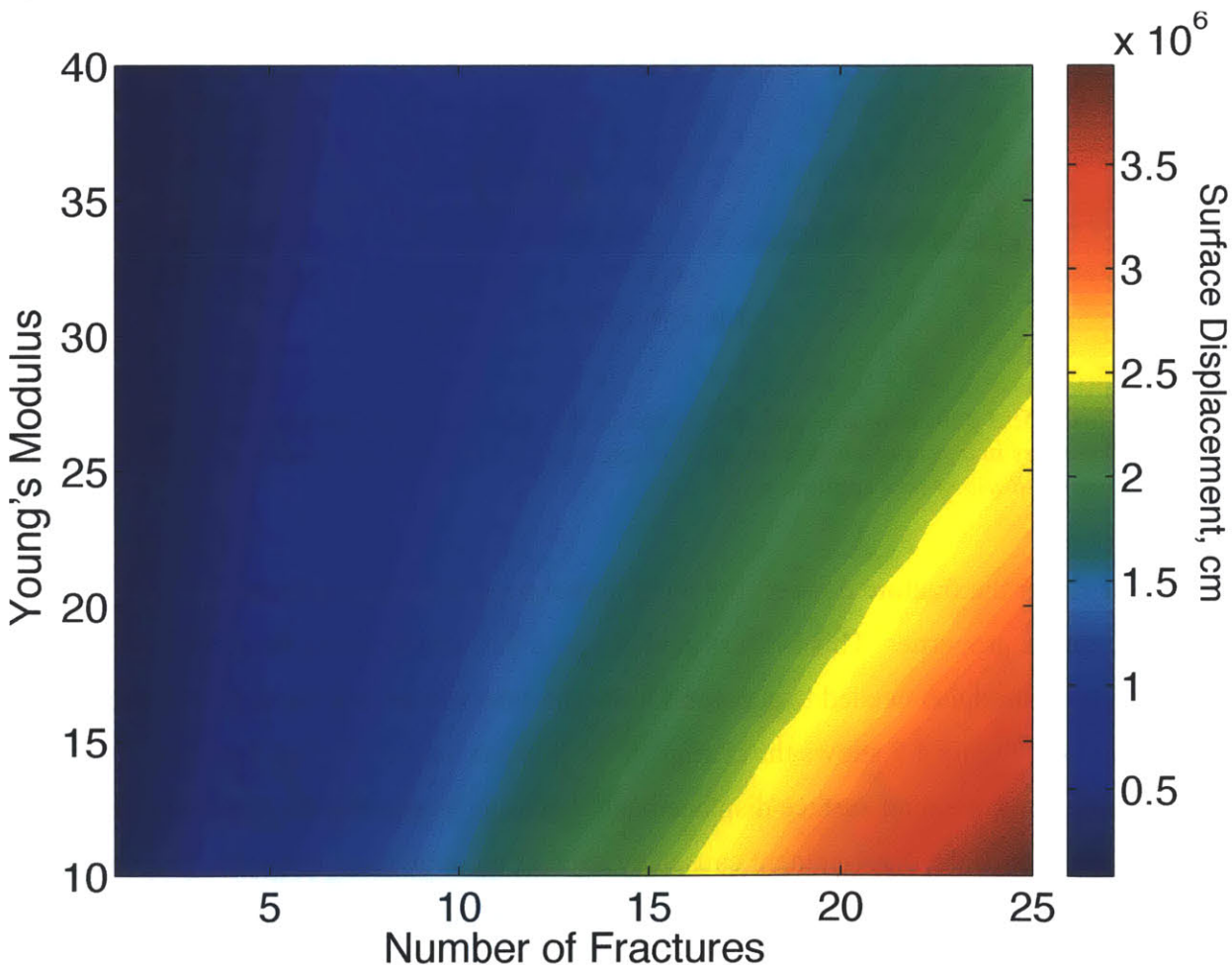


*Figure 4.4: A colormap showing the change in the total surface displacement caused by a group of fractures in a square configuration in a confined region, when the number of fractures and the Young's Modulus of that region are varied.*

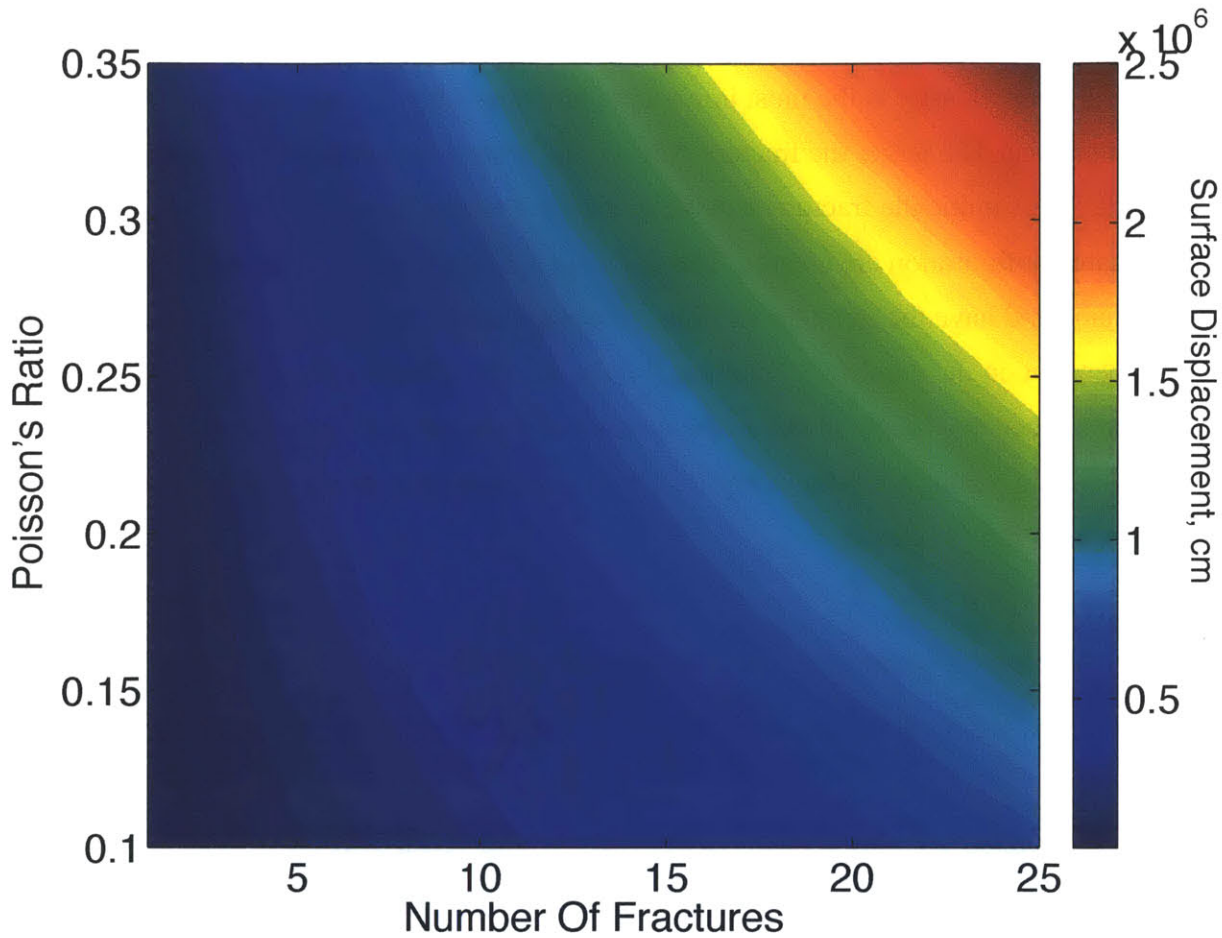


**Figure 4.5:** A colormap showing the change in the total surface displacement caused by a group of fractures in a square configuration in a confined region, when the number of fractures and the Poisson's Ratio of that region are varied.

The larger the fracture density, the more pronounced the effect of fracture interaction on the elastic properties. This is illustrated in figure 4.6, which shows the change in the Young's modulus needed to account for the fracture interactions for different fracture densities. Figure 4.7 shows the change in the Poisson's ratio. To find the effect of fracture interactions, the total surface displacement caused by interacting fractures is normalized by the sum of the displacement caused by each of the individual fractures. The change in surface displacement caused by the interactions for fracture densities with 1, 4, 9, 16, 25, and 36 fractures are found. The interaction effect is then equated with the Young's modulus and Poisson's ratio needed to commeasure the change in surface displacement.

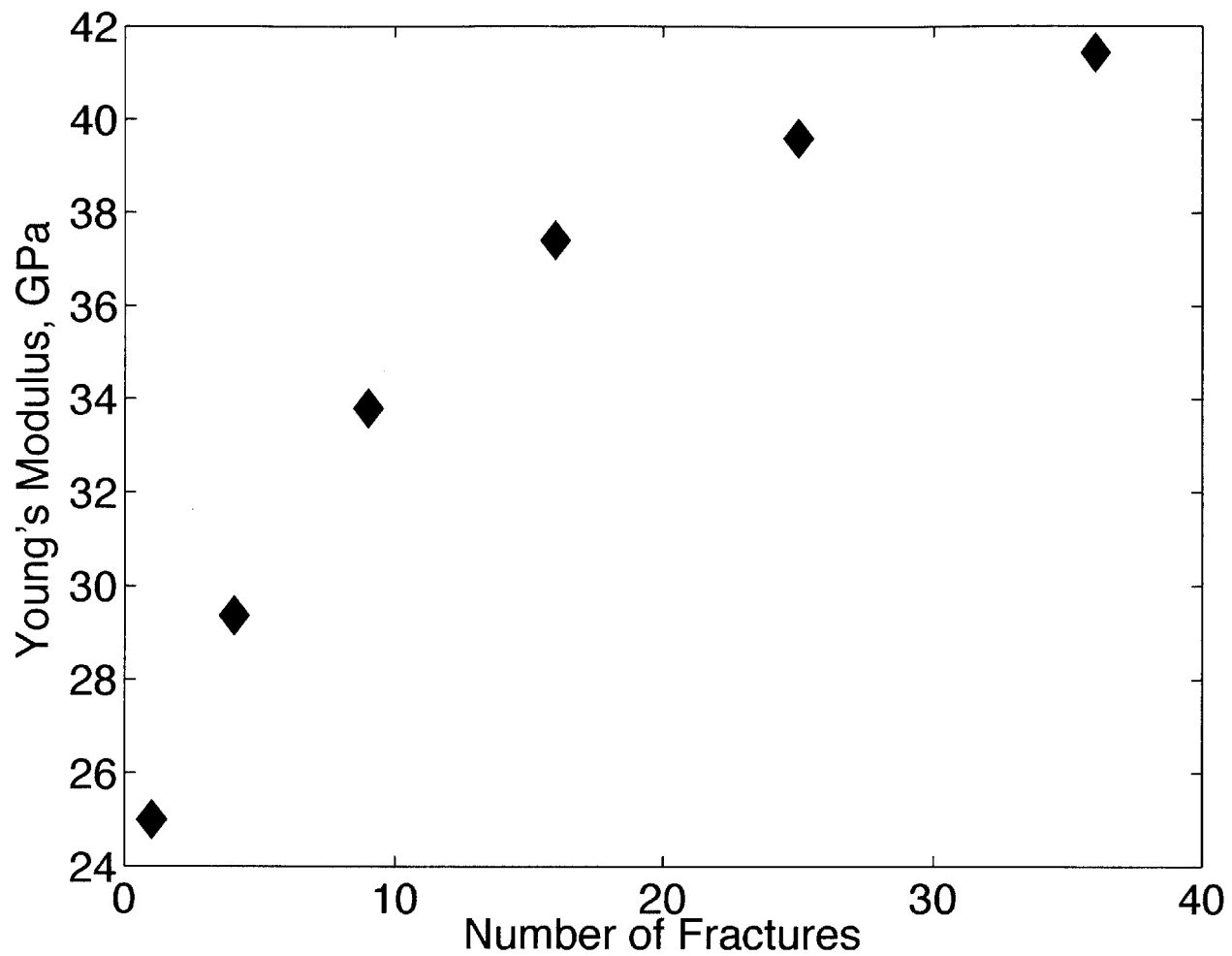


*Figure 4.6: The Young's modulus of the representative volume needed to measure the interaction effect of fractures in a square configuration contained within that volume. The surrounding rock is kept constant at 25 GPa. The value of  $E$  for the interaction effect of a single fracture is therefore 25 GPa.*

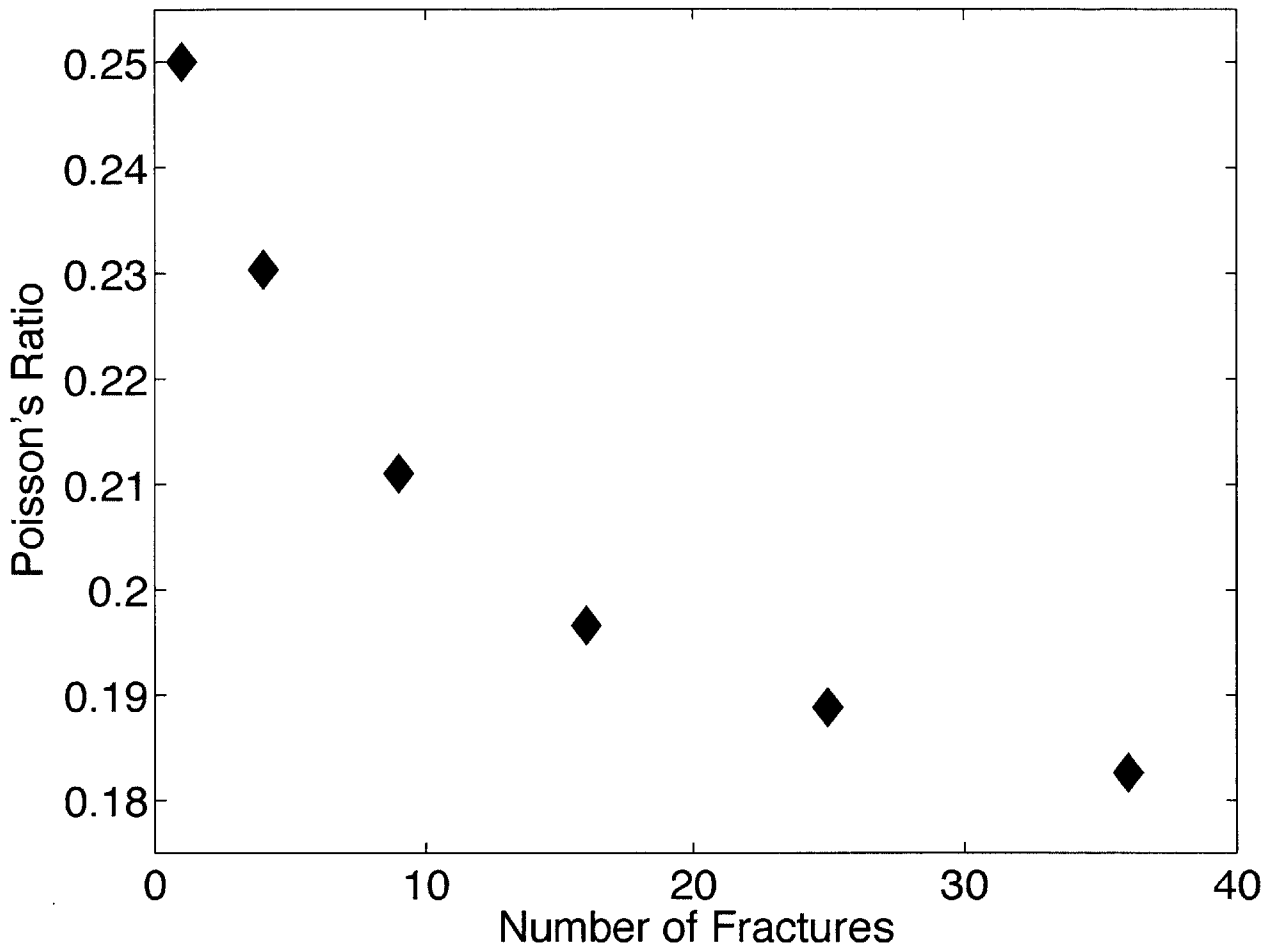


*Figure 4.7: The Poisson's ratio of the representative volume needed to commeasure the interaction effect of fractures in a square configuration contained within that volume. The surrounding rock is kept constant at 0.25. The value of  $v$  for the interaction effect of a single fracture is therefore 0.25.*

## 4.2 Poroelastic Properties of the Representative Volume

From equation 4.3 we can see that the Biot pore-pressure coefficient,  $\alpha$ , relates strain to the pressure change. Rewriting equation 4.3 in terms of the bulk modulus,  $\kappa$ , instead of the shear modulus shows that the strain for a given pressure change is proportional to  $\alpha/\kappa$ . Thus either decreasing  $\alpha$  or increasing  $\kappa$  will decrease the strain for a given pressure change. Here the surface displacement is used as a measure of the strain induced.

The results of section 4.1 show that, as more fractures are inserted into the representative volume, the surface displacement increases, but not at an amount proportional to the number of fractures. The effect of the interaction among fractures is to make the quotient  $\alpha/\kappa$  smaller than it would be if the fractures did not interact. The same effect would occur if the bulk modulus of the representative volume were increased. Thus increasing the modulus of the representative volume can mimic the interaction among fractures.

To explore the poroelastic effect of the elastic properties,  $\kappa$  inside the representative volume is varied from 40 GPa to 80 GPa, while  $\kappa$  in the surrounding rock is held constant at 40 GPa. The same models used in section 4.1 with 1, 4, 9, 16, 25, and 36 fractures are used. The surface displacement caused by the interacting fractures when  $\alpha$  inside the representative volume is equal to that of the surrounding rock is found for the different fracture densities. A plot of the surface displacement vs. fracture density is displayed in red in figure 4.8. On the same graph, the surface displacements vs. fracture density for non-interacting fractures are displayed in black for different values of  $\kappa$  inside the representative volume. In this way we can calculate the change in  $\kappa$  required to represent the surface displacement caused by the interactions of fractures at a given density. At the point where the red line crosses a black line for a given  $\kappa$ , the effect of fracture interactions is the same as the effect of the bulk modulus in the representative volume.

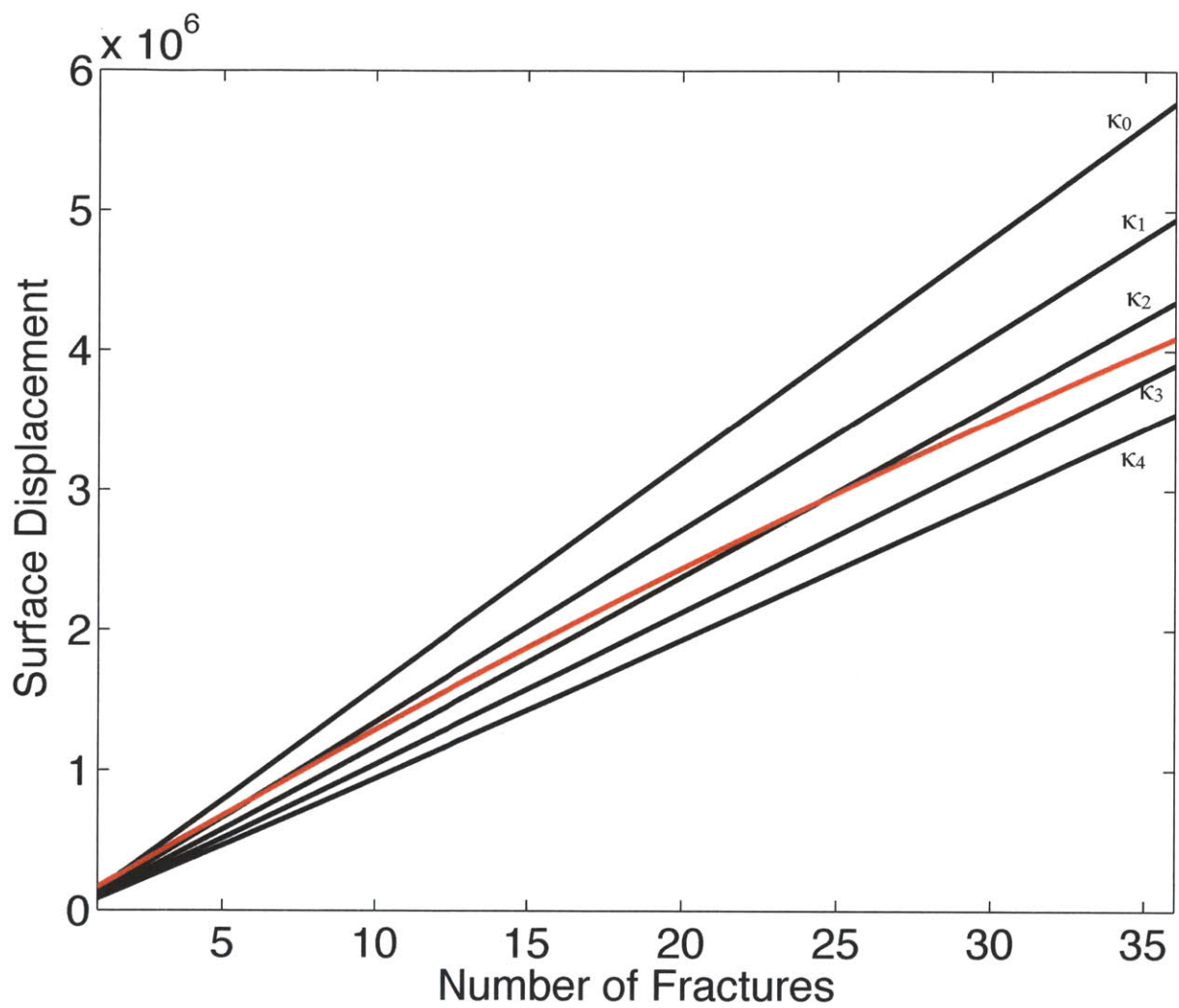


**Figure 4.8:** The change in surface deformation with the fracture density. In red are the results for interacting fractures. The black lines are the results for non-interacting fractures which each have different values of  $\kappa$ .  $\kappa_0$  has the same  $\kappa$  in the representative volume as in the surrounding volume, 40 GPa.  $\kappa_1$  has a  $\kappa$  of 50 GPa,  $\kappa_2$  has a  $\kappa$  of 60 GPa,  $\kappa_3$  has a  $\kappa$  of 70 GPa, and  $\kappa_4$  has a  $\kappa$  of 80 GPa.

### 4.3 Shielding vs. Amplifying Effects

Fracture density is the single most important parameter even when determining the interaction effects, however, the geometric configuration of the fractures is still very important. The net result of interactions is determined by competition between amplification and shielding. When the crack locations are biased towards stacked parallel arrangements, then the shielding effect of interactions dominates, meaning that the overall effective stiffness of a representative volume increases. When collinear interactions dominate then the overall stiffness is reduced. To show this, models with 12 fractures are used and the fracture density is kept constant while the relative positions of the fractures are changed.

The results are seen in figure 4.9. As the domain in the x direction is increased, the domain in the y direction is decreased in such a way that the total volume of the fracture domain is constant. The smaller x direction domains correspond to a larger shielding effect, while the smaller y direction domains correspond to a larger amplifying effect. While this geometry almost always corresponds to a reduction in the total surface deformation, we can see that the configurations which are biased towards the coplanar fracture interactions see a smaller shielding effect. The interaction effect is found by normalizing the total surface displacement induced by the 12 interacting fractures by the sum of the surface displacements induced by each individual fracture. As the fracture configuration becomes more biased towards the shielding effect, the interactions become considerably more damped. This is done by reducing the parallel separation and increasing the coplanar separation between the fractures. The fracture configuration is seen in figure 4.9.

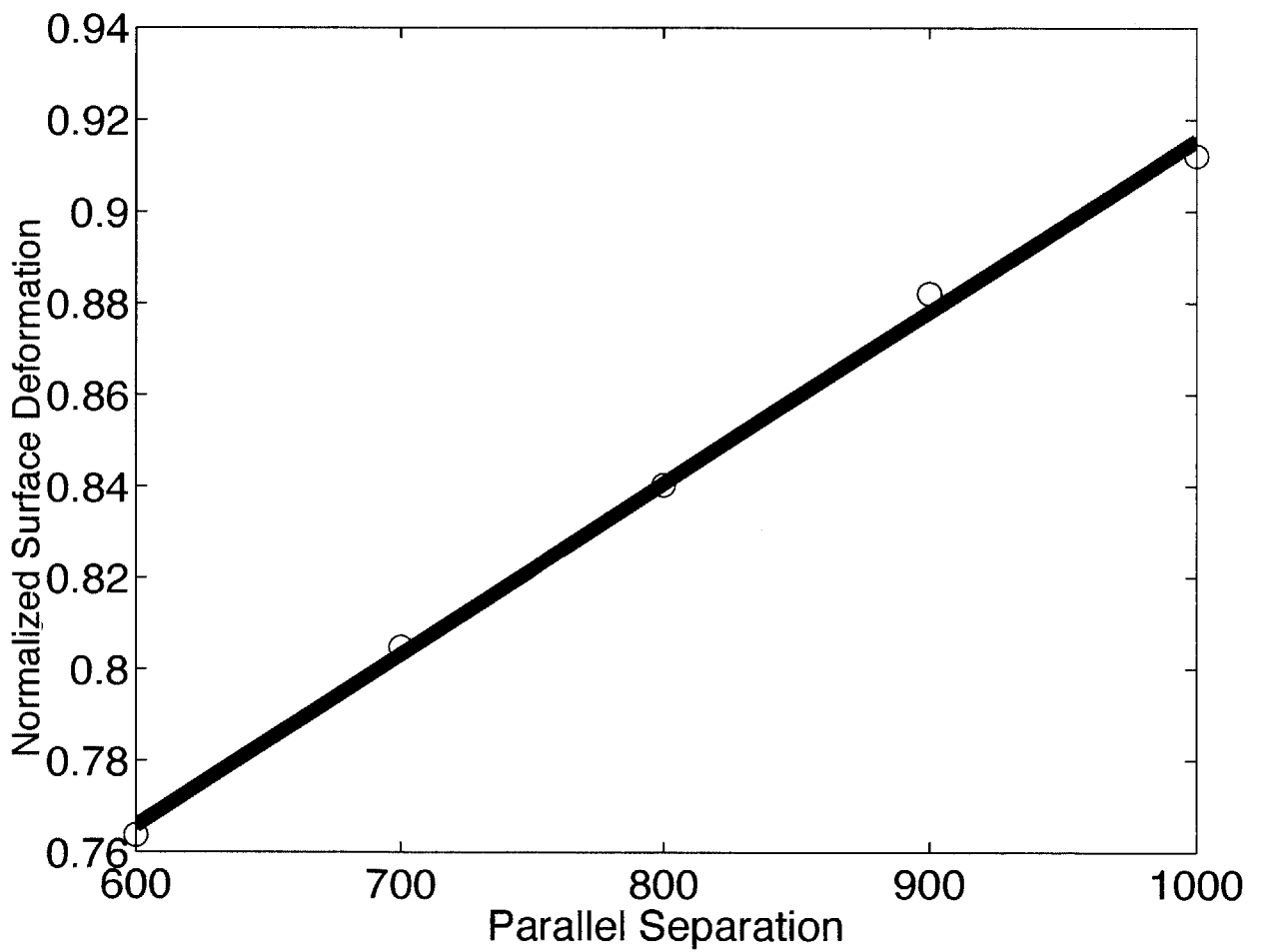
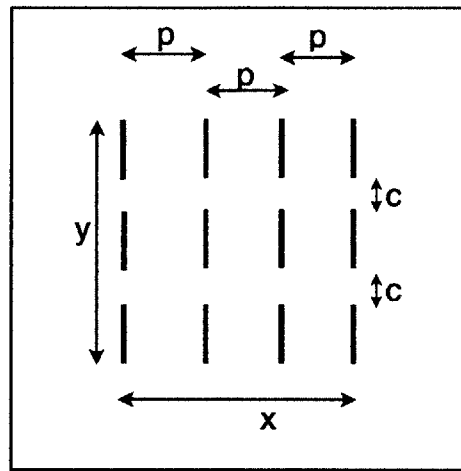


**Figure 4.9:** The change in surface deformation as the fracture configuration is varied from being biased toward parallel fractures to being biased toward coplanar fractures. The total volume,  $xy$  times depth, remains the same throughout. The geometry of the model is shown above where  $p$  is the parallel separation.

#### 4.4 Representative Volume

The size of the representative volume for a given fracture density is an important parameter which must be characterized. To do this, models containing a single fracture in a confined region within a surrounding homogeneous, elastic volume of rock are created. Then, this region has its Young's modulus,  $E$ , and Poisson's ratio,  $v$ , altered in the same manner as before. Now, to find the effect of the volume of the representative region, this region has its volume varied as well. For each volume, the values of  $E$  are varied between 10 and 40 GPa while the surrounding rock has  $E$  of 25 GPa. Then the values of  $v$  are varied from 0.10 to 0.35 while the surrounding rock is held constant at 0.25. A colormap indicating the change in the total surface deformation induced by the fracture in different volumes of different values for  $E$  is seen in figure 4.10. The equivalent colormap for different values of  $v$  is seen in figure 4.11.

The results show that the larger the representative volume, the larger the change in surface displacement. For every volume, as the bulk modulus increases, the surface displacement decreases. When  $E$  is equal to 25 GPa the surface displacement is constant because this setting corresponds to a homogeneous model. When  $E$  is greater than 25 GPa, the larger the representative volume: the smaller the surface displacement. When  $E$  is less than 25 GPa, the larger the representative volume: the larger the surface displacement. This is because for values of  $E$  greater than 25 GPa, the surface displacement is always less than that of the homogeneous model. This means that the effect of increasing the Young's modulus of the representative volume is to decrease the surface deformation. The larger the volume: the larger the decrease. The opposite is true when  $E$  is less than 25 GPa. In this case the surface displacement is greater than that of the homogeneous model, and the decrease in  $E$  creates an increase in displacement, which gets larger as the representative volume increases. The opposite is true for the Poisson's ratio. As the representative volume has a value of  $v$  greater than 0.25, the surface displacement increases as the volume increases. As the representative volume's  $v$  is less than 0.25, the surface displacement decreases as the volume decreases.

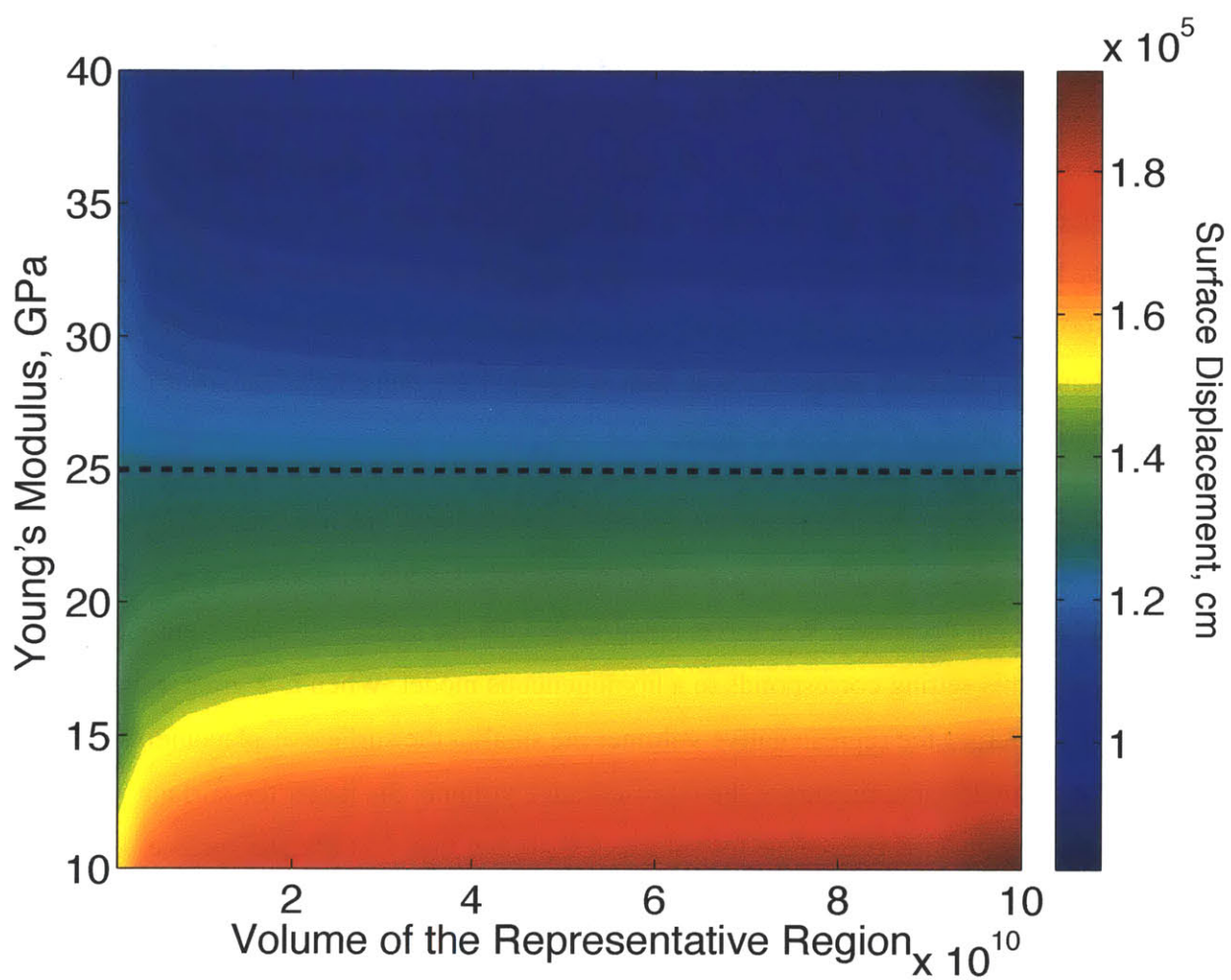


**Figure 4.10** Colormap showing the change in surface displacement with Young's modulus and the volume of the representative rock. The dashed line represents the homogeneous model.

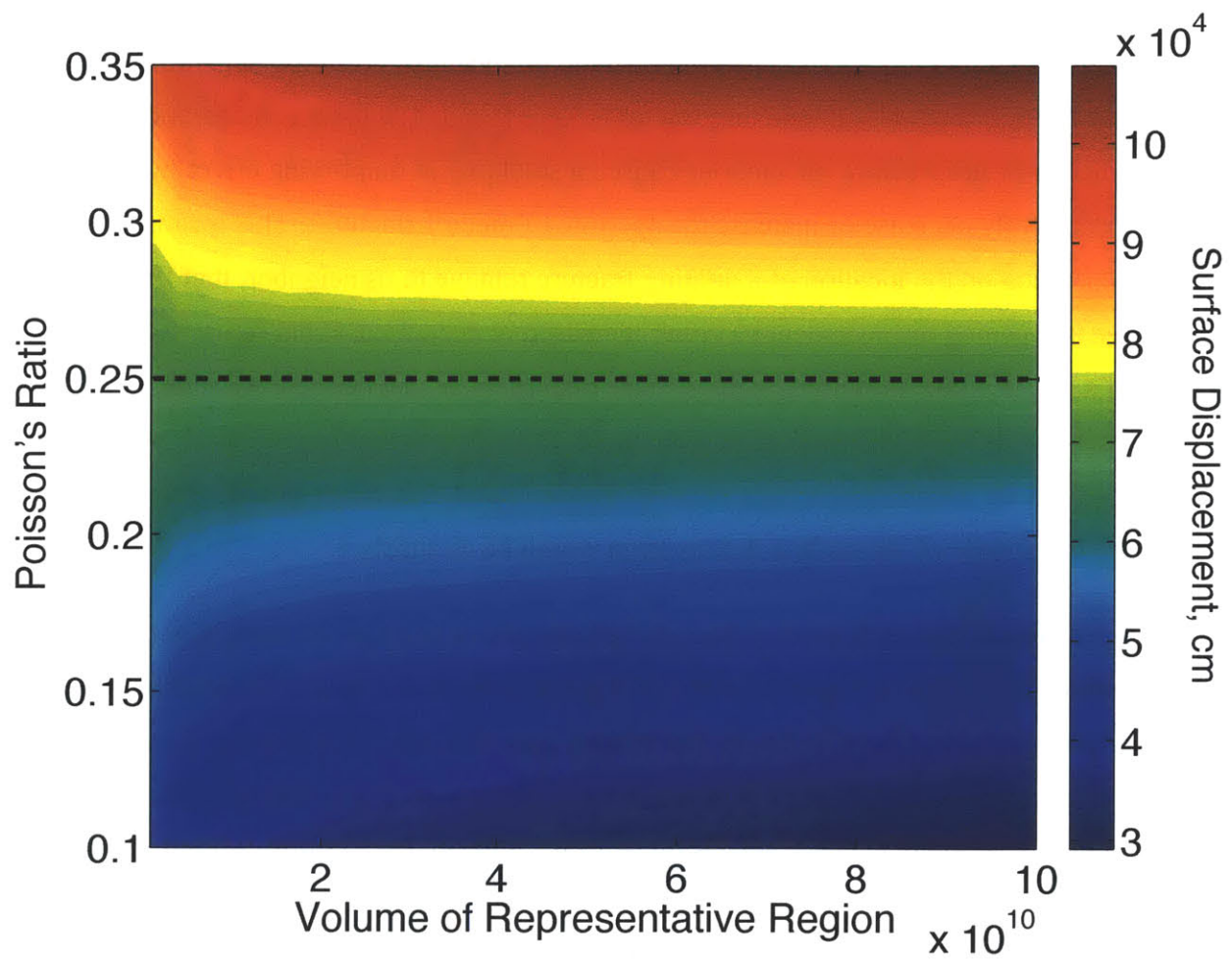


**Figure 4.11:** Colormap showing the change in surface displacement with Poisson's ratio and the volume of the representative rock. The dashed line represents the homogeneous model.

## **Chapter 5**

### **Conclusion**

The effects of stress field interactions of fractures in the subsurface have been characterized in this thesis. The effects of the orientations, positions, separation, areas, and depth of mutually interacting fractures were found. The main consideration was whether or not fracture interactions caused a shielding or amplifying effect, which respectively decrease or increase the aperture of mode 1 fractures. This means that depending on the location of a dilating fracture relative to its neighbor, that fracture could see its opening displacement be either increased or decreased. From figure 1.4, the impact of a single mode 1 fracture on the surface displacement can be seen. As such, if interactions force this fracture to open more, this effect would be increased, while if the interactions decrease its tensile opening displacement, this effect would be decreased and the magnitude of the surface deformation would be diminished.

It was found that each mode 1 fracture had associated stress fields from which one can deduce the locations where its effect is to amplify the stress field of its neighbors and where it shields. Those locations can best be seen in figure 3.1. From this figure it is clear that the shielding zone of a fracture is perpendicular to its plane. The amplification zone is parallel to the plane and radiates outward from its tip. Using this information, two representative geometries can be used to investigate both effects. For the shielding effect, stacked parallel fractures are used, while for the amplifying effect, fractures in the same plane are used. These geometries are intentionally simplified in order to see pure shielding and amplifying effects, not to suggest that those are the only configurations in which fractures occur in nature.

Figures 3.2 and 3.3 show that this formulation is correct as the magnitude of surface deformation change is shielded by parallel fractures and amplified by coplanar fractures. In these geometries there are several important fracture parameters that must be taken into account. The impact of fracture separation is seen in figure 3.4, the impact of fracture area is seen in figure 3.10, and the impact of fracture depth is seen in figure 3.11. The range in which a fracture can influence its neighbors can be seen in figures 3.5 and 3.6.

All of these parameters give a good characterization for individual fractures, but for practical use, this information needs to be extended to see the impact of fractures in a large volume with many fractures. It was found that a solid with many fractures has an additional compliance which reduces its stiffness, but not as rapidly as the increase in the number of fractures. Thus the interaction of fractures causes the material to behave in a less compliant way than it would have if the fractures did not interact. This compliance depends on both the opening displacements of the fractures, and the fracture density. From chapter 3, it is clear that fracture interactions can either reduce or increase the opening displacements of fractures depending on the fracture parameters. Fracture interactions can either reduce or increase this additional compliance, depending on the parameters of those fractures. The overall effect of the fracture density was shown in figures 4.4 and 4.5. Then to show the ability of other fracture parameters to vary the interaction effect, the fracture geometry was changed while the fracture density was held constant (figure 4.8). Figure 4.8 shows clearly that the individual fracture locations are very important when it comes to the overall fracture interactions in a solid with multiple fractures, regardless of fracture density.

With all of this information, it is possible to extend our knowledge of individual fractures to an effective continuum with volume-averaged qualities. In chapter 4, the possibility of replacing a volume of fractured rock with a representative volume with a Young's modulus and a Poisson's ratio that effectively represent the variations due to fracture interactions are considered. This ties into the InSalah problem where the existing models reference a single dilating fracture and do not take the interactions of multiple neighboring fractures into account. It is possible to use the same model with a single dilating fracture but to enhance it by replacing the surrounding fractured rock with a volume with the accurate effective elastic properties. The section 4.3 investigates the importance of the extent of the representative volume on the effective elastic properties.

## **5.1 Future Work**

The impact of individual fracture locations has been outlined throughout chapter 3, however the fracture geometries have been idealized. Configurations other than the coplanar and parallel geometries should be considered. Even though angular changes and oblique fractures have been considered, geometries with different depths and different areas have not been. Additionally, only vertical mode 1 fractures are considered throughout the study, it would be interesting to see the impact of changing the dip of some of these fractures.

In chapter 4, the data from the interaction effect of individual fractures has been extended into an effective continuum with volume average quantities. To conclude this project it should be possible to predict what the change in the effective moduli of the continuum should be, given the information on the fracture locations, orientations, areas, and depths. In this project the effects of each of these parameters has been quantified, both for individual fractures and for the change in bulk modulus required to account for these interactions. The ability to quantify the effects of all of these interrelated parameters should improve the existing models of reservoirs with many fractures.

## Appendix

### A.1 Pylith

The governing equations in Pylith are derived from the Lagrangian description of the conservation of momentum:

$$\frac{\partial}{\partial t} \int_V \rho \frac{\partial^2 u_i}{\partial t^2} dV = \int_V f_i dV + \int_S T_i dS$$

where  $\rho$  = density,  $u$  = displacement,  $T$  = traction,  $f$  = body force, and  $V$  = volume bounded by a surface,  $S$ . By relating traction to the stress tensor, and applying the divergence theorem, several differential equations are found which are conditions which must be met in the finite-element formulation of the elasticity equation.

$$\sigma_{ij,j} + f_i = \rho \frac{\partial^2 u_i}{\partial t^2} \quad \text{in } V$$

$$\sigma_{ij} n_j = T_i \quad \text{on } S_t$$

$$u_i = u_i^0 \quad \text{on } S_u,$$

$$R_{ki} (u_i^+ - u_i^-) = d_k \quad \text{on } S_r$$

$$\sigma_{ij} = \sigma_{ji} \quad (\text{symmetry})$$

where the tractions are specified on the surface  $S_t$ , displacements on the surface  $S_u$ , and slip,  $d_k$ , is specified on the fault surface  $S_r$ .  $R_{ki}$  is the rotation matrix.  $\rho \ddot{u} = f + \nabla \cdot \sigma$  at every location in the volume,  $V$ . To find the finite-element formulation of the elasticity equation, the weak form of the wave equation is constructed using a weighting function,  $\Phi$ , and  $u$  becomes a trial solution which is a piecewise vector field. Now,  $u$  and  $\Phi$  can be expressed as linear combinations of basis functions.

$$u_i = \sum_m a_m^i N^m$$

$$\phi_i = \sum_n c_i^n N^n$$

and then the finite element problem becomes

$$-\int_V \sigma_{ij} N_{,j}^n dV + \int_{S_T} T_i N^n dS + \int_V f_i N^n dV - \int_V \rho \sum_m \ddot{a}_i^m N^m N^n dV = \vec{0}$$

and this equation is solved for the unknown coefficients  $a_i^m$  subject to

$$u_i = u_i^0 \text{ on } S_u \quad R_{ki} (u_i^+ - u_i^-) = d_k \text{ on } S_f$$

For the quasi-static problems, the inertial terms are neglected and so the finite element problem is

$$-\int_V \sigma_{ij} N_{,j}^n dV + \int_{S_T} T_i N^n dS + \int_V f_i N^n dV = \vec{0}$$

considering deformation at time  $t + \Delta t$  the equation is solved through formulation of a linear algebraic system of equations ( $Au - b$ ) involving the residual ( $b - Au$ ) and  $A$  is the Jacobian. Numerical quadrature is employed in the finite-element discretization and the integrals are replaced with sums over the cells and the quadrature points. The mesh containing the cells, quadrature points and the geometry is created using Cubit, a finite-element meshing software. Linear elasticity and infinitesimal strains are approximated using

$$d\sigma_{ij}(t) = C_{ijkl}(t) d\varepsilon_{kl}(t)$$

$C_{ijkl}$  is the 4th order elasticity tensor,  $\varepsilon_{kl}$  is the strain tensor. The models used in this study are three dimensional with dimensions  $8 \text{ km} \times 8 \text{ km} \times 4 \text{ km}$ . They include several two dimensional interfaces which represent fractures. To simulate a dilating mode 1 fracture, an applied traction is imposed on the interface. The stress is extensional, which makes the vertical fractures behave as mode 1 fractures with little slip.

## References

- Aagaard, B., C. Williams, M. Knepley, 2007, PyLith: A finite-element code for modeling quasi-static and dynamic crustal deformation, Eos Trans. AGU, 88(52), Fall Meet. Suppl., Abstract T21B-0592.
- Aagaard, B., C. Williams, M. Knepley, 2008, PyLith: A finite-element code for modeling quasi-static and dynamic crustal deformation, Eos Trans. AGU, 89(53), Fall Meet. Suppl., Abstract T41A-1925.
- Aboudi, J., 1987, Stiffness reduction of cracked solids: Engineering Fracture Mechanics, Vol. 26, No. 5, pp. 637-650.
- Black, N., & Zhdanov, M.S., 2010, Active geophysical monitoring of hydrocarbon reservoirs using EM methods: in J. Kasahara, V. Korneev, and M.S. Zhdanov eds. Active Geophysical Monitoring, Elsevier, 135-159. Published, 03/2010.
- Eiken, O., M. A. Zumberge, T. Stenvold, G. S. Sasagawa, and S. Nooner, 2004, Gravimetric monitoring of gas production from the Troll field: 74th Annual International Meeting, SEG, ExpandedAbstracts, 2243–2246
- Horii, H. and S. Nemat-Nasser, 1885, Elastic Fields of Interacting Inhomogeneities, International Journal of Solids and Structures, 21, No. 7, 731-745.
- Kachanov, M., 1980, Continuum model of medium with cracks: Journal of the Engineering Mechanics Division, ASCE, 106 (EM5), 1039–1051.
- Kachanov, M., 1992, Elastic properties of cracked solids, Critical review of some basic concepts: Applied Mechanics Review, 45, 304-335.
- Kachanov, M., 1993, Elastic solids with many cracks and related problems, in J. W. Hutchinson and T. Wu, eds., Advances in applied mechanics 30: Academic Press Inc, 259-445.
- Lin, J. and R.S. Stein, 2004, Stress triggering in thrust and subduction earthquakes, and stress interaction between the southern San Andreas and nearby thrust and strike-slip faults, J. Geophys. Res., 109, B02303, doi:10.1029/2003JB002607.
- Lumley, D., 2001, Time-lapse seismic reservoir monitoring: Geophysics, 66, 50–53.
- Mathieson, A., Midgely, J., Dodds, K., Wright, I., Ringrose, P., Saoul, N., CO<sub>2</sub> sequestration monitoring and verification technologies applied at Krechba, Algeria Leading Edge, 29 (2010), pp. 216–222
- Nemat-Nasser, S. and M. Taya, 1981, On Effective Moduli of an Elastic Body Containing Periodically Distributed Voids, Quarterly of Applied Mathematics, Vol. 39,

43-59.

O'Connell, R.J., and B. Budiansky, 1976, Seismic Velocities in dry and saturated cracked solids: *Journal of Geophysical Research*, 79, 5412-5426.

Okada, Y., 1992, Internal deformation due to shear and tensile faults in a half-space: *Seismological Society of America Bulletin*, v. 82, p. 1018–1040.

S. Rakes, A. Mathieson & D. Roberts, BP Alternative Energy, P. Ringrose, Integration of 3D Seismic with Satellite Imagery at In Salah CO<sub>2</sub> Sequestration Project, Algeria, SEG Las Vegas 2008 Annual Meeting

Rinaldi, A., Rutqvist, J., 2013, Modeling of deep fracture zone opening and transient ground surface uplift at KB-502 CO<sub>2</sub> injection well, In Salah, Algeria, *International Journal of Greenhouse Gas Control* 12, p. 155-167.

Rutqvist, J., 2010, Coupled reservoir-geomechanical analysis of CO<sub>2</sub> injection and ground deformations at In Salah, Algeria, *International Journal of Greenhouse Gas Control*, doi:10.1016/j.ijggc.2009.10.017, 2009

Toda, S., R. S. Stein, K. Richards-Dinger and S. Bozkurt, 2005, Forecasting the evolution of seismicity in southern California: Animations built on earthquake stress transfer, *J. Geophys. Res.*, B05S16, doi:10.1029/2004JB003415.

Vasco, D. W., A. Ferretti, and F. Novali, F., (2008), Estimating permeability from quasi-static deformation: Temporal variations and arrival-time inversion, *Geophysics* 73, O37-O52.

Vasco, D.W., Rucci, A., Ferretti, A., Novali, F., Bissell, R.C., Ringrose, P.S., Mathieson, A.S., Wright, I.W., 2010. Satellite-based measurements of surface deformation reveal fluid flow associated with the geological storage of carbon dioxide. *Geophys. Res. Lett.* 37

Williams, C.A., B. Aagaard, M.G. Knepley, 2005, Development of software for studying earthquakes across multiple spatial and temporal scales by coupling quasi-static and dynamic simulations, *Eos Trans. AGU*, 86(52), Fall Meet. Suppl., Abstract S53A-1072.

Williams, C.A., 2006, Development of a package for modeling stress in the lithosphere, *Eos Trans. AGU*, 87(36), Jt. Assem. Suppl., Abstract T24A-01 Invited.